# 2022 年臺灣國際科學展覽會
# 優勝作品專輯

作品編號　**100042**

參展科別　工程學

作品名稱　**What is the relationship between angular velocity and power efficiency of a twin blanded single rotor helicopter system, in hover?**

得獎獎項　四等獎


國　　家　**Norway**

就讀學校　**International School of Stavanger**

指導教師　**Lynn Parker**

作者姓名　**Omkar Patil**



關鍵詞　**Angular velocity and power efficiency of twin bladed single rotor helicopter system**

# 作者照片

## 1.0 Introduction

Helicopters are used for their ability to take off and land vertically, qualifying them for a host of tasks, namely: tourism, aerial observation, and medical transportation (“Helicopter Career Info”, 2017). An intriguing physics phenomenon of a helicopter is its potential to hover. A twin bladed single rotor helicopter consumes 60 - 85% more power to hover than with forward flight, making the extremely manoeuvre inefficient (Lombardi, 2017). A vast amount of literature has been published for optimising blade shape and fuselage weight to enhance efficiency. However, the role of a rotors angular velocity has never been addressed. Hence, this essay attempts to answer the question “What is the relationship between angular velocity and power efficiency of a twin bladed single rotor helicopter system, in hover?”

The essay seeks to correct Froude's momentum and Drzweicki’s blade element theory, to obtain a theoretical model for power efficiency in terms of angular velocity. In order to test the validity of the theoretical model, an experiment is devised to evaluate the correlation between the theoretical and empirical power data. Firstly, the essay delves into Froude's model and realises the necessity of thrust and power coefficient in expressing power efficiency. To accommodate the NACA 0015 aerofoil geometry used within this experiment, these coefficients are corrected by integrating small blade elements along the blade using Drzewiecki's model. Thereafter, a dependence between air resistance and thrust coefficient is established and incorporated using XFOIL simulations. The simulation allows to compare thrust and power coefficient against angular velocity with industrial specifications, providing insights into hypothetically inefficient, ideal, and efficient ranges for power in terms of angular velocity.

Correspondingly, the absolute uncertainty for coefficients is found to be substantially large, losing confidence with the theoretical model. Hence, to affirm if the investigation is concurrent with empirical data, an experiment is devised to simulate a helicopter rotor, obtaining data for power coefficient. The empirical and theoretical power coefficient establish a strong correlation, which implied the uncertainties accumulated as a consequence of extensive mathematical calculations. Ultimately, the calculated coefficients were substituted in the model, yielding a clear relationship between power efficiency and angular velocity. This research question is worthy of investigation, as it advances the understanding and provides impetus to the research in power performance of aerial crafts. Commercially, we observe the demand of various clients including airlines and hobbyists who desire to minimise battery drain time and maximise usage, leading to the central question of power efficiency.

## 2.0 Background Information

Power dissipated is the product of force imparted on air and mean air velocity. In order to establish a theoretical model for power efficiency, we therefore require inspecting airflow velocity and the different forces acting on a rotor system.

A hovering helicopter is considered at rest since the body has zero acceleration and so zero net-force. The airscrew of a twin bladed single rotor helicopter rotates around a central z-axis, propelling air in a downwards vortex known as the slipstream, Figure 1. The slipstream is governed by an inverse relationship termed the venturi effect, where the decreasing cross-sectional area ($A$), increases air velocity ($\bar{v}$) (Halliday et al., 2014). In the early 20$^{\text{th}}$ century, William Froude combined venturi effect with Bernoulli's principle; formulating an equation for the axial force (z-plane) lifting a helicopter - thrust ($T$).

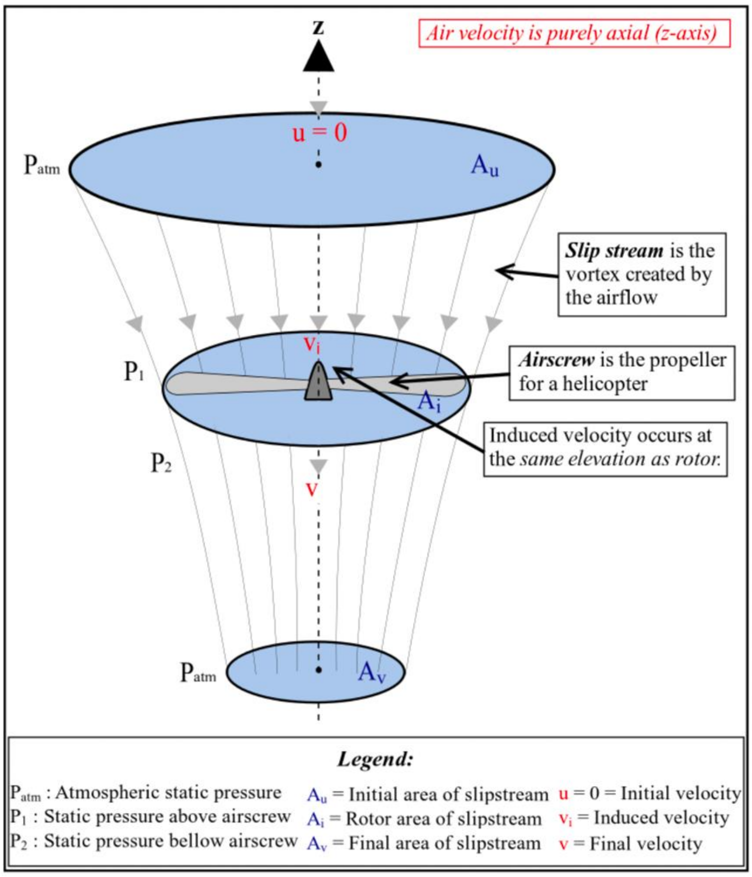


**Figure 1:** A slipstream for twin bladed single rotor helicopter.

According to Bernoulli's principle, the rotor system experiences dynamic pressure ($P_d$) inside and static pressure ($P_s$) outside the slipstream boundary, which always adds to a constant (1). The dynamic pressure characteristically exhibits proportionality with airflow velocity: $P_d \propto \bar{v}$ (Zhao et al., 2019). We assume air density is $\rho = 1.23\ kgm^{-3}$ for simplicity, although the value varies with elevation.

$$\Sigma P = P_s + P_d = \text{constant}$$

$$\Sigma P = P_s + \frac{1}{2}\rho\overline{v^2} = \text{constant} \tag{1}$$

The airflow velocity increases along slipstream from initial velocity ($u = 0\ ms^{-1}$) above to final velocity ($v$) below the airscrew, proportionally increasing dynamic pressure. Therefore, the cross-sectional area decreases from $A_u$ above to $A_v$ below the airscrew by the venturi effect, proportionally decreasing static pressure from $P_1$to $P_2$ respectively, preserving the constant relationship in (1).

$$\text{Above airscrew: } \Sigma P = P_1 + \frac{1}{2}\rho u^2$$

$$\text{Bellow airscrew: } \Sigma P = P_2 + \frac{1}{2}\rho v^2$$

$$P_1 + \frac{1}{2}\rho u^2 = P_2 + \frac{1}{2}\rho v^2$$

Then rearranging the equation to find pressure differential experienced by the airscrew, we have

$$P_1 - P_2 = \frac{1}{2}\rho(u^2 - v^2)$$

$$\text{Dynamic pressure differential: } \Delta P_d = P_2 - P_1 = \frac{1}{2}\rho v^2 \qquad (\text{Since, } u = 0\text{ms}^{-1})$$

### 2.1 Induced velocity and thrust:

Froude argued, since pressure is the quotient of net-force and cross-sectional area, a greater dynamic pressure beneath the blade causes an upwards directed net-force, Figure 2. This net-force is termed thrust, acting orthogonal to airflow on the airscrew (2) (Venkatesan, 2012). The airscrew area is assumed to be circular where blade's radius is $R$, denoted by $A_i = \pi R^2$.

$$\Sigma \text{Force}_{net} = P_d(A_i)$$

$$T = \frac{1}{2}A_i \rho v^2$$

$$T = \frac{1}{2}\rho\pi R^2 v^2 \tag{2}$$

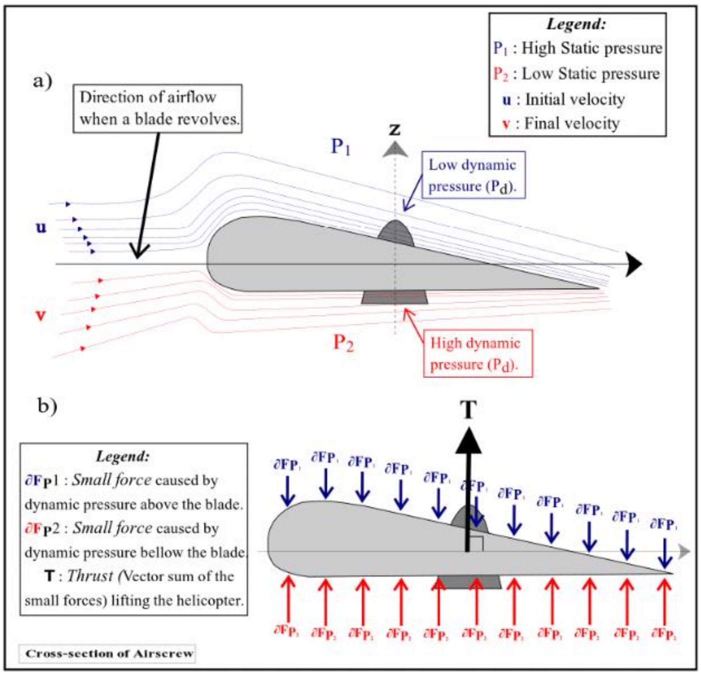


**Figure 2:** Froude uses Bernoulli's principle and properties of venturi effect to model thrust ($T$) in a rotor system.

Conversely, Froude proposed an alternative argument where air particles are the frame of reference. Air particles have negligible mass, requiring mass flow rate ($\dot{m}$) defined as the fluid mass passing the airscrew per unit time. Mass can also be considered as volumetric density ($m = V\rho$), where velocity of air positioned at the rotor is known as induced velocity ($v_i$).

$$\dot{m} = \frac{\Delta m}{\Delta t}$$

$$\dot{m} = \frac{V\rho}{t} \implies \dot{m} = \rho A_i v_i$$

Elastic collision occurs between air particles and airscrew for conserving momentum in the system, producing an equal and opposite axial thrust force (Gessow & Myers, 1985). Substituting $\dot{m}$ in Newton's second law, we obtain thrust (3). We assume ideal gas properties are preserved in such high-pressure situations for simplicity.

$$\mathrm{F} = \mathrm{ma} \implies F = \dot{\mathrm{m}}(\Delta\bar{\mathrm{v}})$$

$$T = \rho A_i v_i (v - u)$$

$$T = \rho\pi R^2 v_i v \quad (Since, u = 0ms^{-1}) \tag{3}$$

Realising (2) and (3) model thrust and incorporate similar variables except for velocity, equating the two expressions yields an important velocity identity (4).

$$T = \rho\pi R^2 v_i v = \frac{1}{2}\rho\pi R^2 v^2$$

$$2v_i = v \tag{4}$$

Thereby, substituting this velocity identity within (2) and (3), we may derive a unified thrust equation (5). Moreover, by isolating induced velocity we determine an equation for velocity at the airscrew (6). This model for force and velocity is Froude's momentum theory (Gessow & Myers, 1985).

$$T = \rho\pi R^2 v_i (2v_i) = \frac{1}{2}\rho\pi R^2 (2v_i)^2$$

$$T = 2\rho\pi R^2 v_i^2 \tag{5}$$

$$v_i = \sqrt{\frac{T}{2\rho\pi R^2}} \tag{6}$$

**2.2 Power and power efficiency:**

Recalling from earlier, power ($\bar{P}$) can now be defined as the product of axial thrust force orthogonal to airflow and induced air velocity shown in (7).

$$\bar{P} = Fv \implies Tv_i \quad (7)$$

Power efficiency is the ratio between useful and total power, expressed in percentage. In fluid mechanics, useful power is represented by (7), as here the fluid behaves in an ideal system without viscosity. Viscosity measures a fluids resistance to deformation (Adminstration, 2020). Total power refers to power measured experimentally ($\overline{P_{exp}}$), where aerodynamic losses due to resistive forces are considered. Hence, expanding for power efficiency yields (8).

$$\eta = \frac{\text{Useful Power}}{\text{Total Power}} \times 100 \implies \eta = \frac{Tv_i}{\overline{P_{exp}}} \times 100 \quad (8)$$

The exploration in deriving power efficiency has laid the foundation for this essay. This foundation allows incorporating the important concept of angular velocity.

## 3.0 Extending Power Efficiency

Investigations in fluid mechanical systems incorporate coefficients, as they allow simplifying power performance equations (Gessow & Myers, 1985). The thrust coefficient ($c_T$) recognises the ratio between total thrust produced and cross-sectional area (9). Similarly, power coefficient recognises the ratio between power required and cross-sectional area (9). These coefficients recognise blade velocity in circular motion, $v_{blade} = \omega R$, where ω represents the blade's angular velocity. Also notice, these equations are non-dimensional and thus have no unit.

$$\text{Thrust coefficient: } T = c_T \rho\pi R^2(\omega R)^2 \qquad \text{Power coefficient: } \bar{P} = c_P \rho\pi R^2(\omega R)^3$$

$$c_T = \frac{T}{\rho\pi R^2(\omega R)^2} \qquad c_P = \frac{\bar{P}}{\rho\pi R^2(\omega R)^3} \quad (9)$$

In order to substitute the coefficients for power efficiency, we first require expressing induced velocity in terms of the coefficients. Therefore, induced velocity from (6) simplifies to (10).

$$v_i = \sqrt{\frac{T}{2\rho\pi R^2}} = \sqrt{\frac{c_T \rho\pi R^2(\omega R)^2}{2\rho\pi R^2}}$$

$$v_i = \omega R\sqrt{\frac{c_T}{2}} \quad (10)$$

Substituting induced velocity from (10), thrust and power coefficient all in (8), we obtain a simplified form for power efficiency (11).

$$\eta = \sqrt{\frac{c_T^3}{2c_P^2}} \times 100 = 70.7 \times \frac{c_T^{\frac{3}{2}}}{c_P} \quad (11)$$

The sections hereafter are based on calculating thrust and power coefficients to determine a relationship between power efficiency and angular velocity (ω).

## 4.0 Slipstream Correction for Pitch Angle

Pitch angle/ pitch (θ) refers to the angle a blade makes with the horizontal (x-axis). Empirical analysis confirms, thrust cannot be produced without pitch (Venkatesan, 2012). Unified thrust in (5) assumes a zero-pitch system and so fails to satisfy the properties that change with pitch. These properties are illustrated in Figure 3 and Table 1.

**Table 1:** Properties that change in a system when implementing a blade pitch angle

| Properties changed | Description |
|---|---|
| Angular velocity ($\omega$) | A blade rotating through air, is similar to air flowing across a stationary blade with angular velocity ($\omega$) and tangential velocity ($\omega r$), depending on the radial position of blade ($r$). |
| Inflow velocity ($v_i$ and $\omega r$) | Along with induced velocity (z-plane), air also has tangential velocity: $\omega r$ (x-y plane). The vector sum of velocities is resultant velocity, $v_R$ (12). |

$$v_R = \sqrt{v_i^2 + (\omega r)^2} \tag{12}$$

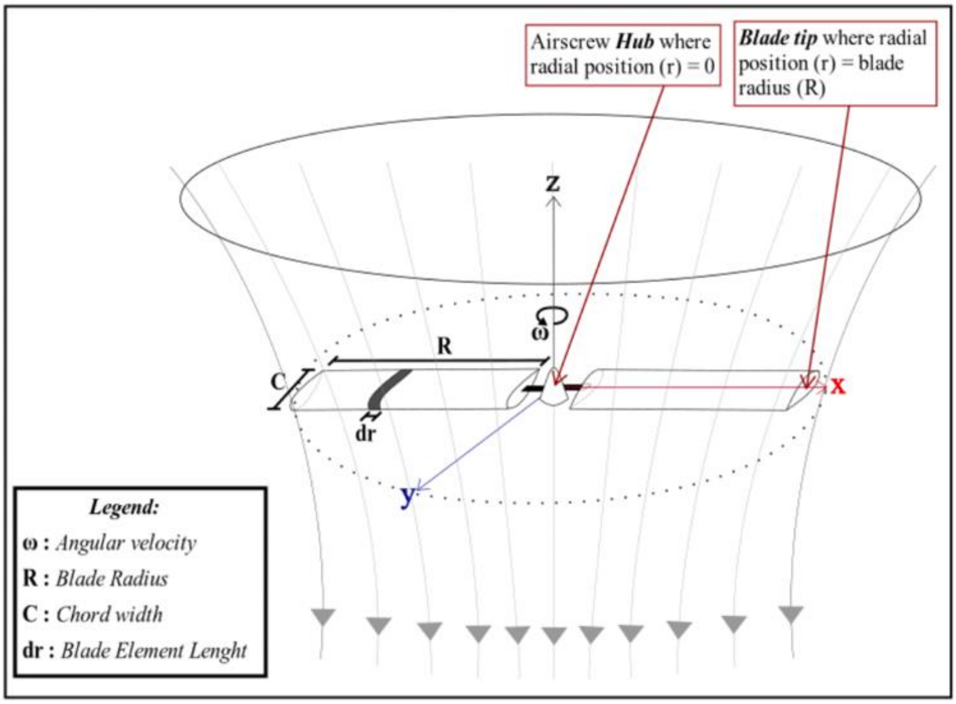


**Figure 3:** A modified approach to the slipstream model.

Due to these properties, pitch comprises of inflow angle of attack (Inflow AoA (ϕ)) and angle of attack (AoA (α)), demonstrated in Figure 4 and (13). The inequality $\theta > \phi$ and $\theta > \alpha$ holds true, hence by the small angle approximation, the quotient of induced and tangential velocity $\tan \phi$ is approximately equal to ϕ (14). As inflow AoA is small, so is induced velocity and therefore resultant velocity in (12) is best approximated by tangential velocity (15).

$$\theta = \phi + \alpha \tag{13}$$

$$\tan\phi = \frac{v_i}{\omega r} \approx \phi \tag{14}$$

$$v_R \approx \omega r \tag{15}$$

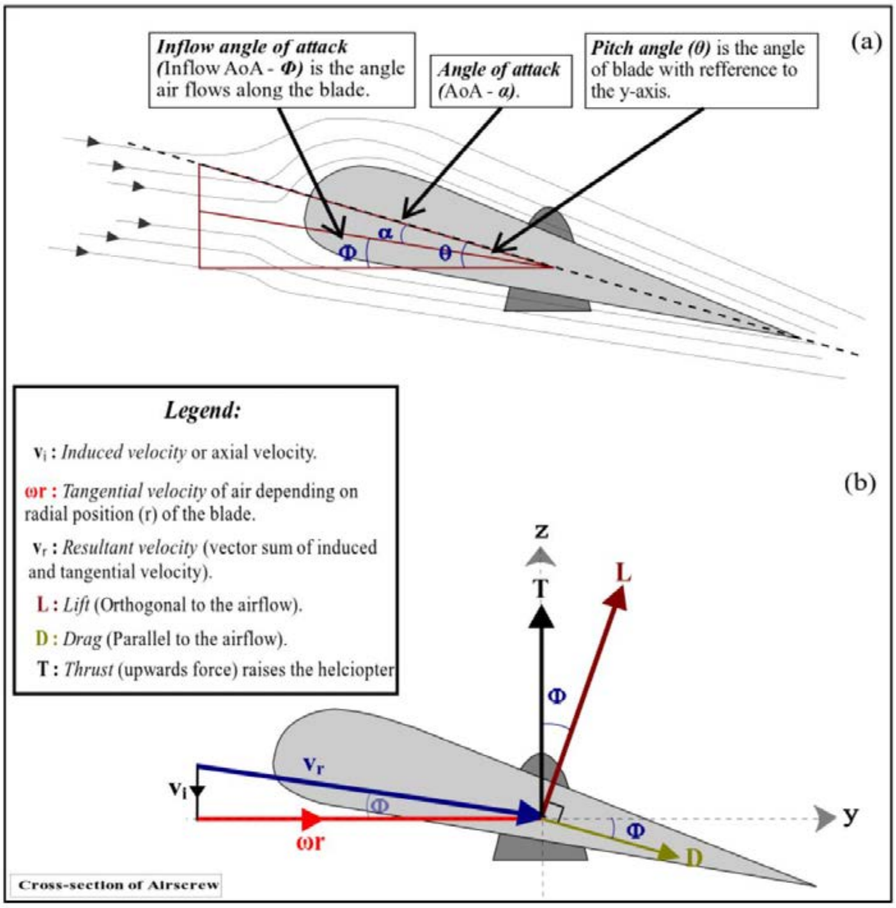


**Figure 4:** A diagram in which (a) deconstructs the angles in relation with the blades, (b) interprets the blades free body diagram.

The force perpendicular to airflow is lift ($L$) and a new force parallel to airflow also exists, termed drag ($D$), Figure 4. The vertical component of lift and drag produces thrust. As the inflow AoA is insignificant ($\phi \approx 0$), trigonometric ratios reduce to $\cos\phi \to 1$ and $\sin\phi \to 0$. Hence, thrust approximately equals lift (16).

$$T = L\cos\phi + D\sin\phi$$

$$T \approx L \tag{16}$$

## 5.0 Determining Thrust Coefficient

Realise, the force orthogonal to airflow is lift, corresponding with Bernoulli's principle (2)

$$L = \frac{1}{2}A\rho\overline{v^2}$$

Substituting resultant velocity (15) in lift, we recognise as radial position ($r$) increases from hub ($r = 0$) to tip ($r = R$), lift also increases with each blade element ($dr$). This implies lift is non-uniformly produced along the blade. The blade element theory suggests, the cumulative sum of all blade elements is total lift and hence we use integration (Gessow & Myers, 1985). Furthermore, the blade element area is rectangular and therefore product of infinitesimal length ($dr$) and chord width ($C$) shown in Figure 3.

$$L = \int_0^R \frac{1}{2} C\rho(\omega r)^2 \, dr$$

Incorporating an empirical factor known as the lift coefficient ($c_L$) allows accounting for the NACA 0015 aerofoil geometry used in our experiment (see section 7). The lift coefficient is a first order function when mapped with AoA ($\alpha$) and passes through origin $(\alpha, c_L)\colon (0,0)$ (Venkatesan, 2012). The function is $y = mx \Leftrightarrow c_L = a\alpha$, where '$a$' is the lift-curve gradient. We make AoA subject of (13) and further substitute inflow AoA (14) for lift.

$$L = \int_0^R \frac{1}{2} C\rho(\omega r)^2 \, c_L dr = \int_0^R \frac{1}{2} C\rho(\omega r)^2 \, a\alpha dr$$

$$\alpha = \theta - \phi \implies \alpha = \theta - \frac{v_i}{\omega r}$$

$$L = \int_0^R \frac{1}{2} C\rho(\omega r)^2 \, a\left(\theta - \frac{v_i}{\omega r}\right) dr$$

We simplify lift and remove constants outside the integral. Since, lift only considers force from one blade, multiplying by 2 yields total lift. As lift-thrust identity (16) holds true, total lift approximates thrust (17).

$$L = \frac{1}{2} C\rho a \int_0^R \theta(\omega r)^2 - v_i(\omega r) dr$$

$$T = C\rho a \int_0^R \theta(\omega r)^2 - v_i(\omega r) dr \tag{17}$$

Lastly, we can now determine the corrected thrust coefficient using (9), by substituting for the corrected thrust (17). Realise by dividing the fraction, we obtain a new variable, $\bar{r} = \frac{r}{R}$ (Venkatesan, 2012). Hence, boundary conditions change; lower limit $\lim_{r\to 0} \bar{r} = 0$ and upper limit $\lim_{r\to R} \bar{r} = 1$.

$$c_T = \frac{T}{\rho\pi R^2(\omega R)^2} \implies \frac{C\rho a \int_0^R \theta(\omega r)^2 - v_i(\omega r) dr}{\rho\pi R^2(\omega R)^2}$$

$$c_T = \frac{Ca}{\pi R} \int_0^1 \left(\theta(\bar{r})^2 - \frac{v_i}{\omega R}(\bar{r})\right) d\bar{r}$$

To further simplify, we assume inflow AoA $\phi = \frac{v_i}{\omega r} \approx \frac{v_i}{\omega R}$. This assumption is valid as magnitude for tangential velocity along the blade ($\omega r$) approximates to that at the tip ($\omega R$), since dynamic pressure is significantly larger at the tip, due to the proportionality between dynamic pressure and radial position. Substituting this approximation and solving the integral we obtain the thrust coefficient (18).

$$c_T = \frac{Ca}{\pi R}\int_0^1 (\theta\overline{r^2} - \phi\bar{r})d\bar{r} = \frac{Ca}{\pi R}\left[\frac{\theta\overline{r^3}}{3} - \frac{\phi\overline{r^2}}{2}\right]_0^1$$

$$c_T = \frac{Ca}{\pi R}\left(\frac{\theta}{3} - \frac{\phi}{2}\right) \tag{18}$$

Since, chord width ($C = 0.0180 \pm 0.00500m$), radius of blade ($R = 0.0900 \pm 0.00500m$) and pitch ($\theta = 0.157 \pm 0.00900rad$) are measured variables in the experiment (see section 7), we require to know inflow angle of attack and lift-curve gradient to determine thrust coefficient.

### 5.1 Determining inflow angle of attack:

We still assume $\phi = \frac{v_i}{\omega r} \approx \frac{v_i}{\omega R}$ to keep inflow AoA constant with radial position, otherwise the investigation becomes convoluted. Notice, (10) from section 3 can be rearranged to the form $\frac{v_i}{\omega R}$, which by our assumption approximates to the inflow AoA.

$$v_i = \omega R\sqrt{\frac{c_T}{2}} \Rightarrow \phi \approx \frac{v_i}{\omega R} = \sqrt{\frac{c_T}{2}}$$

Substituting for thrust coefficient (18) and lift-curve gradient, $a = 2\pi$ (explained in section 5.2), we express inflow AoA as a quadratic.

$$\phi^2 = \frac{c_T}{2} = \frac{Ca}{2\pi R}\left(\frac{\theta}{3} - \frac{\phi}{2}\right)$$

$$\left(\frac{R}{C}\right)\phi^2 + \left(\frac{1}{2}\right)\phi - \frac{\theta}{3} = 0$$

Replacing values measured in experiment (see section 7) forms a quadratic (19).

$$5.00\phi^2 + 0.500\phi - 0.0520 = 0 \tag{19}$$

The steps for error propagation are demonstrated bellow.

| | |
|---|---|
| Fractional uncertainty for numerator.<br>Fractional uncertainty for denominator.<br>Sum of fractional uncertainties for numerator and denominator is that for coefficient of $\phi^2$.<br>Absolute uncertainty for coefficient, rounded to 3.sig.fig. | $\frac{\Delta R}{R} = \frac{0.00500}{0.0900} = 0.0560m$<br>$\frac{\Delta C}{C} = \frac{0.00500}{0.0180} = 0.278m$<br>$\frac{\Delta R}{R} + \frac{\Delta C}{C} = 0.334$<br>$\Delta\frac{R}{C} = 1.70m$ |
| Fractional uncertainty for y-intercept equals fractional uncertainty for pitch.<br>Absolute uncertainty for y-intercept is rounded to 3.sig.fig similar to y-intercept. | $\frac{\Delta\theta}{\theta} = \frac{0.00900}{0.157} = 0.0573m$<br>$\Delta\frac{\theta}{3} = 0.00300m$ |

$$(5.00 \pm 0.170)\phi^2 + 0.500\phi - (0.0520 \pm 0.00300) = 0$$

We obtain an original, maximum, minimum value for inflow AoA after implementing the uncertainties and graphically solve them in the domain $(0, \infty)$. The original quadratic (19) yields $\phi = 0.0640 rad$ (Figure 5a).

$$5.00\phi^2 + 0.500\phi - 0.0520 = 0$$

The maximum quadratic yields $\phi = 0.0740 rad$ (Figure 5b).

$$5.00\phi^2 + 0.500\phi - 0.0520 = 0$$

The minimum quadratic yields $\phi = 0.0560 rad$ (Figure 5c).

$$6.70\phi^2 + 0.500\phi - 0.0550 = 0$$

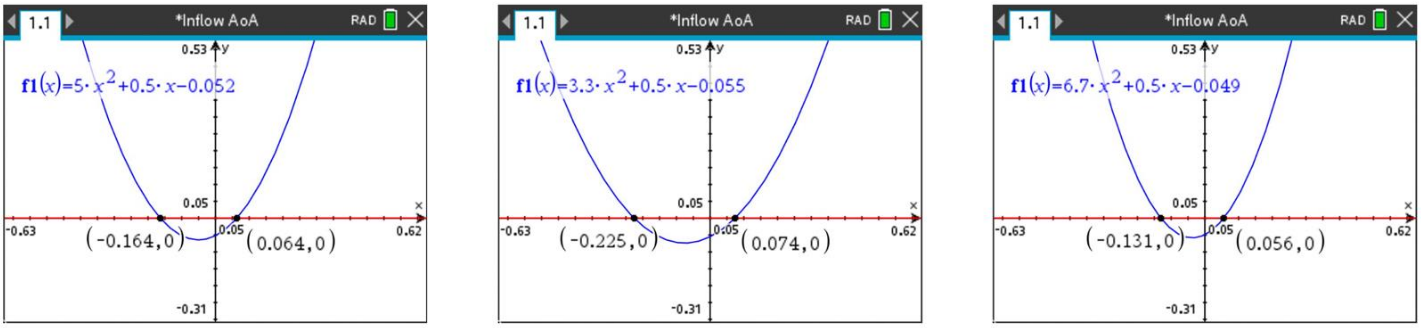


**(a)** $y = (5.00)\phi^2 + (0.500)\phi - (0.0520) = 0$ **(b)** $y = (3.30)\phi^2 + (0.500)\phi - (0.0490) = 0$ **(c)** $y = (6.70)\phi^2 + (0.500)\phi - (0.0550) = 0$

**Figure 5:** Graphs to determine inflow AoA ($\phi$).

Hence, a good approximation for inflow AoA is the mean ($\overline{\phi}$) of range and for uncertainty is unbiased standard deviation ($\sigma_\phi$) demonstrated below.

$$\overline{\phi} = \frac{\phi_1 + \phi_2 + \phi_3}{3} = \frac{0.056 + 0.064 + 0.074}{3} = 0.0650$$

$$\sigma_\phi = \sqrt{\frac{(\phi_1 - \overline{\phi})^2 + (\phi_2 - \overline{\phi})^2 + (\phi_3 - \overline{\phi})^2}{N - 1}}$$

$$\sigma_\phi = \sqrt{\frac{(0.056 - 0.065)^2 + (0.064 - 0.065)^2 + (0.074 - 0.065)^2}{2}} = 0.00903$$

Therefore, inflow AoA, $\phi = 0.0650 \pm 0.00903$ to 3.sig.fig.

### 5.2 Determining lift-curve gradient:

The lift-curve gradient accounts for resistive forces caused by the blade's (aerofoil) geometry. Air resistance results from skin friction and form drag creating turbulence, Figure 6. Turbulence decreases tangential velocity, proportionally decreasing dynamic pressure (Administration, 2020). By Froude's argument this decreases thrust.

The industrially averaged magnitude for lift-curve gradient is $a = 2\pi$, for all angular velocities and aerofoil (Scott, 2018). The lift-curve gradient of lift coefficient against AoA ($c_L$ vs ) graph can be found using XFOIL; a fluid simulation programme. XFOIL develops a unique environment for varying angular velocities of a rotor based on Reynolds number (Re), which predicts airflow patterns (Halliday et al., 2014). After undergoing a mathematical process (see Appendix 1), Reynolds number is found using simplified form (20).

$$Re = 1266.98(\omega R) \tag{20}$$

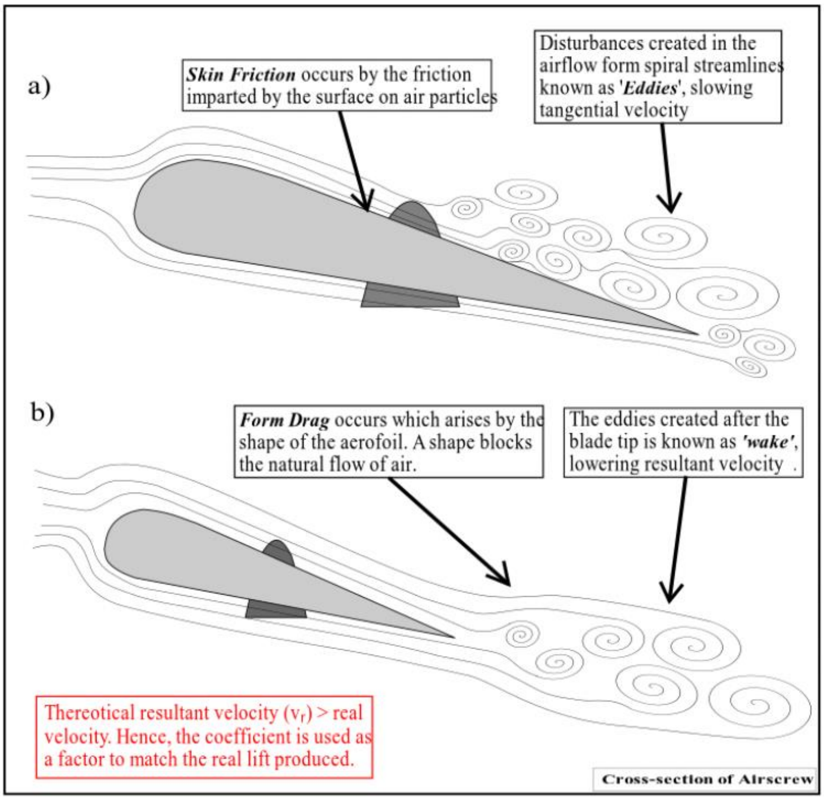


**Figure 6:** Air resistance forces which occur decreasing resultant velocity.

To determine Reynolds number, we require to define angular velocities to simulate in XFOIL. The experiment in section 7, uses revolutions per minute ($RPM\ min^{-1}$) as a relative measure for angular velocity. The experiment uses a motor with an operational range from $0 - 7000\ RPM$, where tests are conducted in increments of $250\ RPM$. We will therefore simulate within the operational range and the same increments. RPM determines frequency of revolution, hence conversion to angular velocity requires conversion factor $\frac{2\pi}{60}$. A sample set of conversions is shown in Table 2, where values are rounded to $RPM$ of lowest significant figure. Substituting angular velocities, we obtain Reynolds numbers displayed in sample Table 2 (see Appendix 2). Error propagation is unnecessary as XFOIL does not recognise error, decreasing the confidence in lift-curve gradient.

**Table 2:** A table determining Reynolds number

| Revolutions per minute ($RPM$) | Angular velocity ($\omega$) | Tangential velocity ($\omega R$) | Reynolds Number ($Re$) |
|---|---|---|---|
| $/min^{-}$**Table 3:** A table determining lift-curve gradient | | | - |
| 0 | 0 | 0 | 0 |
| 250 | 26 | 2.4 | 3000 |
| 500 | 50 | 5 | 6000 |
| 750 | 79 | 7.1 | 9000 |
| 1000 | 100 | 10 | 10000 |
| ... | ... | ... | ... |

Reporting Reynolds number to XFOIL, a simulation is produced in one tab (see Figure 7a) and a $c_L$ vs α table in the other. The table is then converted to a graph (see Figure 7b), which uses 26 $rads^{-1}$ as an example. A linear regression line is graphed to verify linearity, which as indicated by the Pearson correlation coefficient $r = 0.998$ is very strong. However, a systematic error is observed as the regression line intersects the y-axis at $(\alpha, c_L)$: $(0, -0.007)$, but not the origin. The difference between y-intercepts is negligible, hence the graph can be considered reliable. The lift-curve gradient for $26rads^{-1}$ is $a = 1.47$ to 3.sig.fig. The remaining angular velocities are found similarly, shown in sample Table 3 (see Appendix 3).

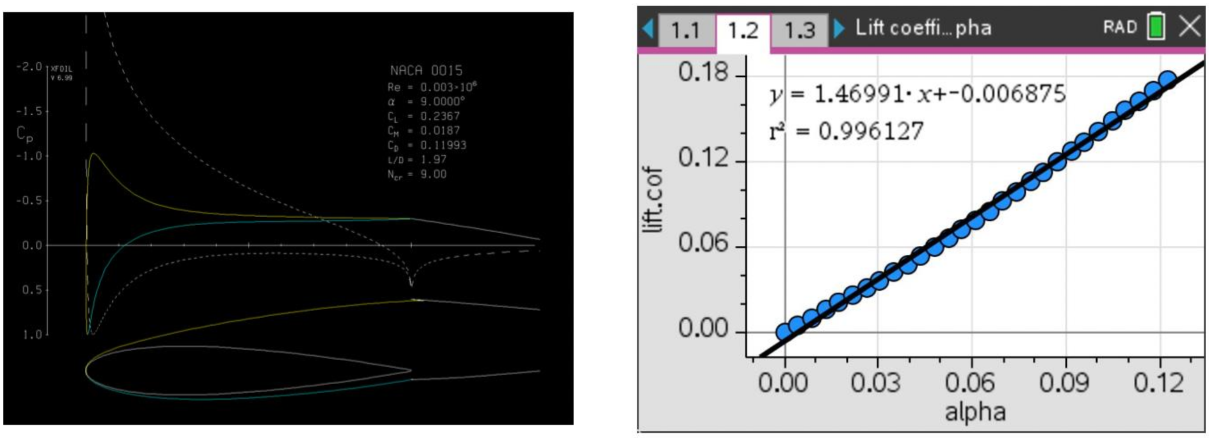


**(a)** An illustration of XFOIL simulation for $26rads^{-1}$.

**(b)** A lift $c_L$ vs $\alpha^c$ graph.

**Figure 7:** Simulation and analysis of data from XFOIL.

**Table 3:** A table determining lift-curve gradient

| Angular velocity ($\omega$) | Tangential velocity ($\omega R$) | Reynolds Number ($Re$) | Lift-curve gradient ($a$) |
|---|---|---|---|
| $/rad\ s^{-1}$ | $/m\ s^{-1}$ | - | - |
| 0 | 0 | 0 | 0 |
| 26 | 2.4 | 3000 | 1.47 |
| 50 | 5 | 6000 | 1.28 |
| 79 | 7.1 | 9000 | 1.23 |
| 100 | 10 | 10000 | 1.22 |
| ... | ... | ... | ... |

Data from Table 3 is quantitatively demonstrated as a graph in Figure 8. The mean for all lift-curve gradient points is represented as a mean line ($a_{theo} = 4.81$). An industrially agreed mean line is also illustrated

($a_{emp} = 2\pi = 6.28$). The data points $< a_{theo}$ $(0 - 222 rads^{-1})$ shows a theoretically inefficient range, as a great proportion of work is lost to turbulence, which decreases dynamic pressure. Similarly, data points between $a_{theo}$ and $a_{emp}$ $(222 - 240 rads^{-1}$ and $431 - 733 rads^{-1})$ indicates an ideal range, as predominant amount of work is used to generate thrust. Lastly, data points $> a_{emp}$ $(240 - 431 rads^{-1})$ represents an efficient range, as resistive forces insignificantly impact dynamic pressure and therefore, most work generates thrust.

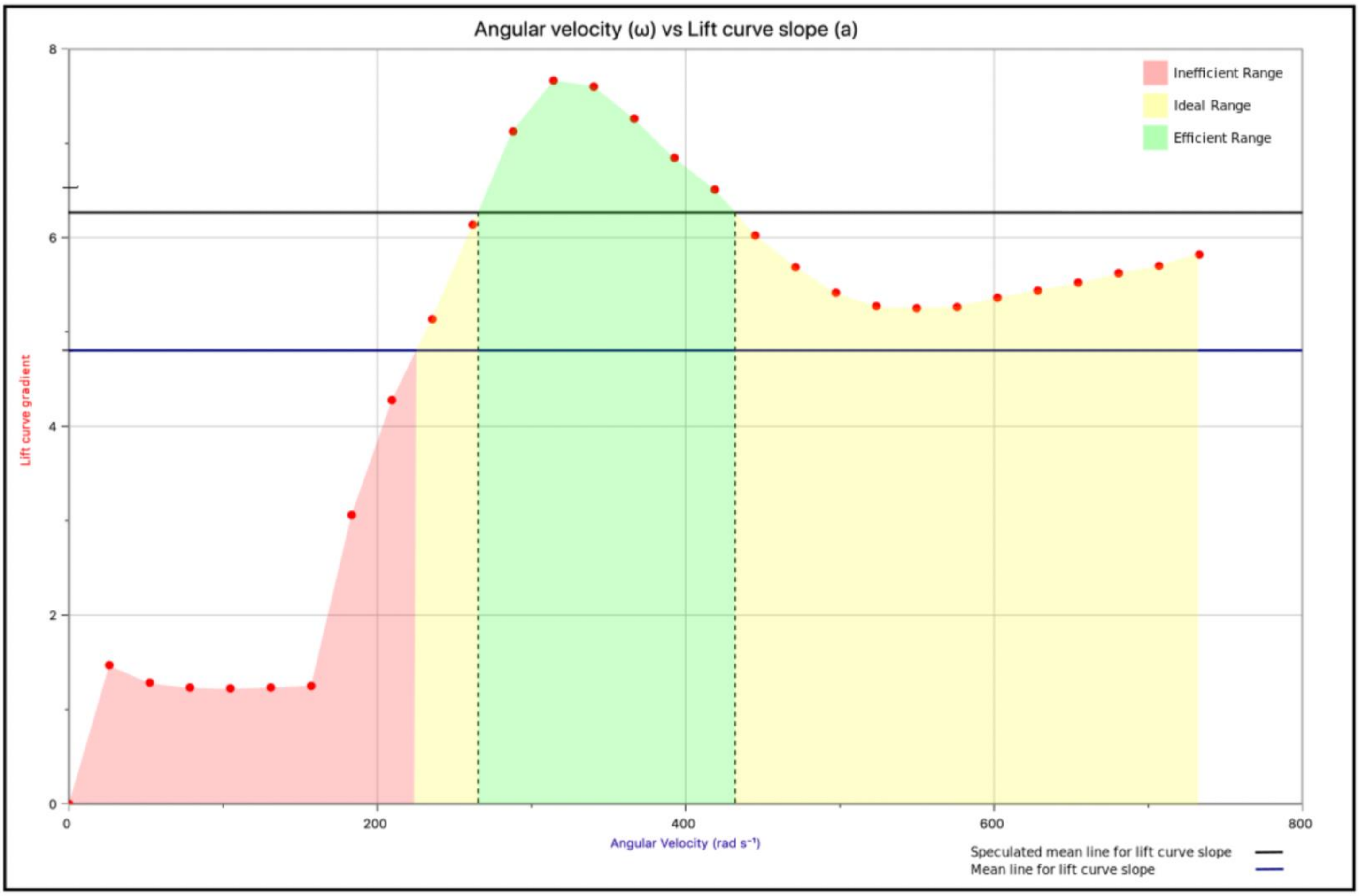


**Figure 8:** The relationship between angular velocity and lift-curve gradient.

### 5.3 Determining thrust coefficient:

Recalling (18), we can now find the thrust coefficient with respect to angular velocity. However, the thrust coefficient is theoretically deduced and fails to recognise mechanical losses for e.g. bearing friction. This requires to implement a constant $k = 1.75$ (Venkatesan, 2012).

$$c_T = k\frac{Ca}{\pi R}\left(\frac{\theta}{3} - \frac{\phi}{2}\right)$$

Substituting values for the variable's, we obtain thrust coefficient demonstrated in Table4 (see Appendix 4). The thrust coefficient is calculated to 3.sig.fig, as the variable with smallest significant figure.

Uncertainty for the thrust coefficient are found with steps bellow.

| | |
|---|---|
| Fractional uncertainty for multiplicand ($\frac{Ca}{\pi R}$) is that for $\frac{C}{R}$, as other variables have zero uncertainty. | $\frac{\Delta \frac{Ca}{\pi R}}{\frac{Ca}{\pi R}} = 0.334$ derived from section 5.1. |
| Fractional uncertainty for $\frac{\theta}{3}$ is that for pitch. | $\frac{\Delta\theta}{\theta} = \frac{0.00900}{0.157} = 0.0573$ |
| Absolute uncertainty for $\frac{\theta}{3}$. | $\Delta\frac{\theta}{3} = 0.00300$ |
| Same steps for absolute uncertainty of $\frac{\phi}{2}$. | $\Delta\frac{\phi}{2} = 0.00400$ |
| Absolute uncertainty for $\frac{\theta}{3} - \frac{\phi}{2}$. | $\Delta\frac{\theta}{3} - \frac{\phi}{2} = 0.00300 + 0.00400 = 0.00700$ |
| Fractional uncertainty for multiplier. | $\frac{\Delta\frac{\theta}{3}-\frac{\phi}{2}}{\frac{\theta}{3}-\frac{\phi}{2}} = \frac{0.00700}{0.0200} = 0.350$ |
| Fractional uncertainty for thrust coefficient is sum of the fractional uncertainty for multiplicand and multiplier. | $\frac{\Delta c_T}{c_T} = 0.334 + 0.350 = 0.684$ |
| Percentage uncertainty for thrust coefficient | $\Delta c_T\% = 68.4\%$ |

**Table 4:** A table demonstrating the thrust coefficient $c_T$ based on it's constituent angular velocity ($\omega$).

| **Air screw geometry ($R$, $C$)** | **Air screw angles ($\theta$, $\phi$)** | **Angular velocity ($\omega$)** | **Lift-curve gradient ($a$)** | **Thrust coefficient ($c_T$)** |
|---|---|---|---|---|
| $/m$ | $/rad$ | $/rad\ s^{-1}$ | - | - |
| $\pm0.00500, \pm0.00500$ | $\pm0.00900, \pm0.00900$ | - | - | 68.4% |
| 0.0900, 0.0180 | 0.157, 0.0650 | 0 | 0 | 0 |
| | | 26 | 1.47 | 0.00359 |
| | | 50 | 1.28 | 0.00313 |
| | | 79 | 1.23 | 0.00301 |
| | | 100 | 1.22 | 0.00299 |
| | | ... | ... | ... |

The data from Table 4 is quantitatively represented as a graph in Figure 9. The trend closely corresponds with lift-curve gradient against angular velocity graph in Figure 8. The mean of all thrust coefficient data points is illustrated with a mean line. Although error bars are substantially large, the inefficient range is positioned below the mean line and the opposite is true for ideal and efficient ranges providing confidence with our speculations.

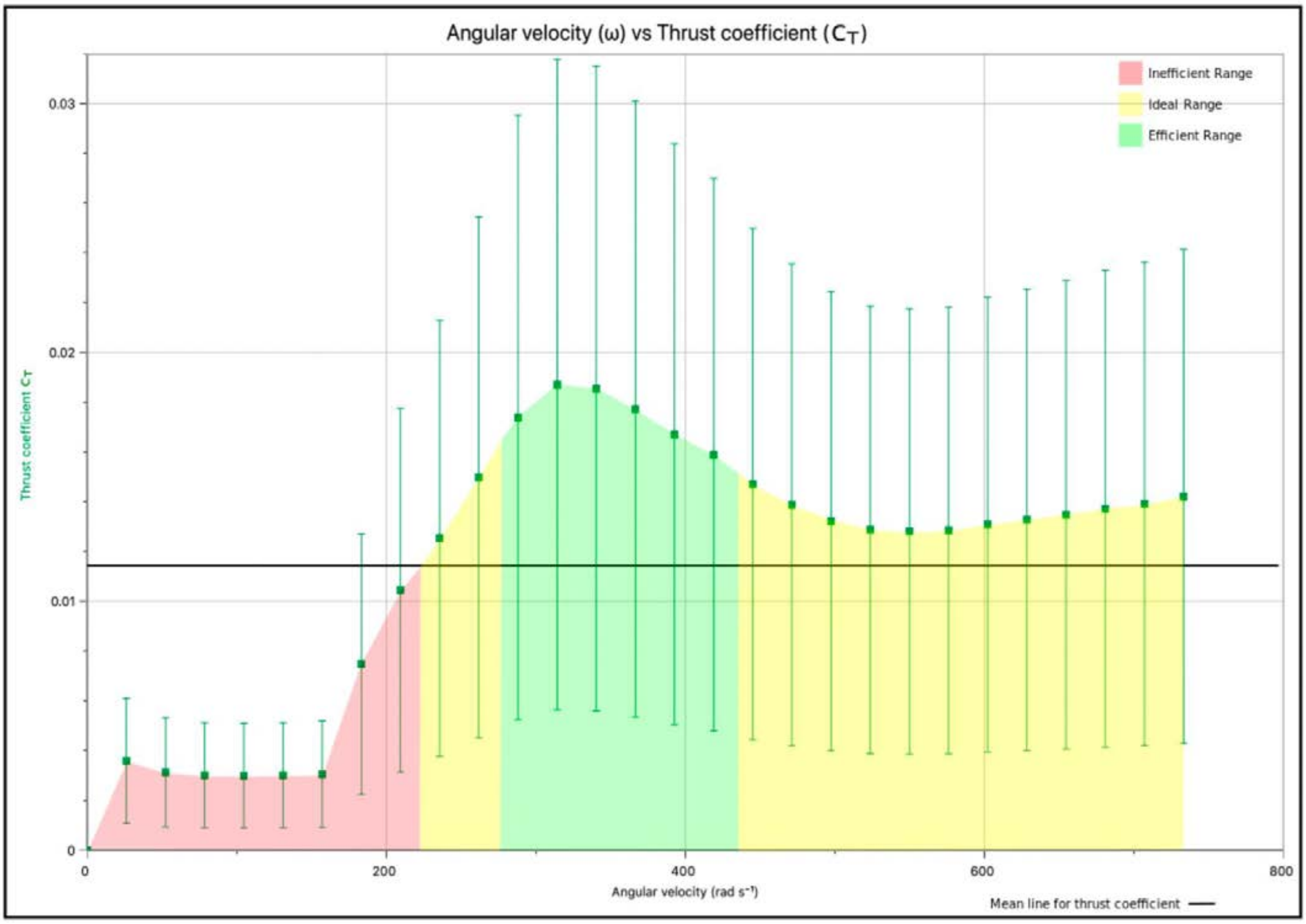


**Figure 9:** The relationship between angular velocity and thrust coefficient.

## 6.0 Determining Power Coefficient

The power determined in (7) is unsatisfactory, as it omits variables such as, resultant velocity and air resistance. Hence, we may consider a new approach, which focuses on the revolution of an airscrew. Power is tangential force ($F$) experienced by an aerofoil along a distance ($s$) divided by some time elapsed ($\Delta t$) to travel the distance (see Figure 10a).

$$\bar{P} = Fv = \frac{Fs}{\Delta t}$$

The magnitude of arc length travelled can be expressed as $s = \beta R$, where the aerofoil revolves an angle β in $\Delta t$ time. Notice, $\frac{\beta}{\Delta t}$ is the definition of angular velocity. Power is therefore the product of tangential force and velocity.

$$\bar{P} = \frac{F\beta R}{\Delta t} = F(\omega R)$$

Additionally, considering air as the frame of reference, tangential force is the horizontal component of lift and drag, Figure 10b. The small angle approximation for inflow AoA simplifies $\sin\phi \rightarrow \phi$ and $\cos\phi \rightarrow 1$. Lift and drag may be expanded using the blade element theory by integrating along the blade's length. The expanded expression for drag is equivalent to lift except for the drag coefficient ($c_D$) (Gessow & Myers, 1985).

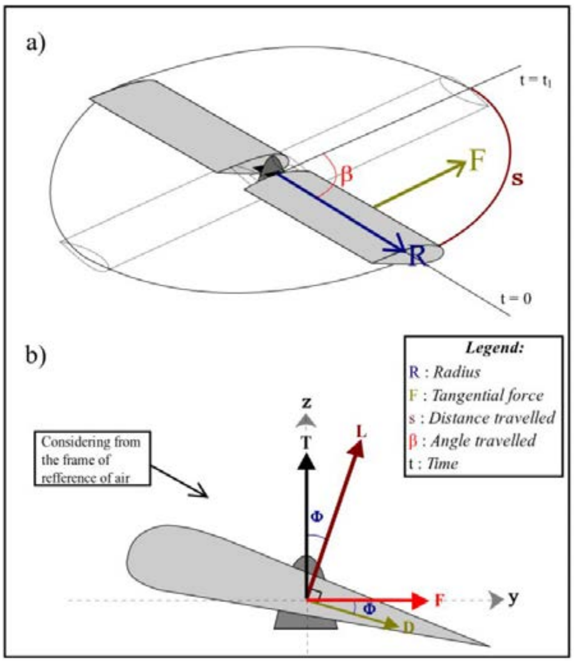


**Figure 10:** A modified approach for power coefficient.

$$\bar{P} = \omega R \left[\int_0^R (L\sin\phi + D\cos\phi)dr\right] = \omega R \int_0^R (L\phi + D)dr$$

$$\bar{P} = \omega R \int_0^R \left(\frac{1}{2}C\rho(\omega r)^2 c_L\right)\phi dr + \int_0^R \frac{1}{2}C\rho(\omega r)^2\, c_D dr$$

$$\bar{P} = \frac{1}{2}C\rho\omega R\left[a\phi\int_0^R \theta(\omega r)^2 - v_i(\omega r)dr + \int_0^R (\omega r)^2\, c_D dr\right]$$

We multiply the power equation by two, in order to consider both blades (21). Substituting power within the power coefficient from (9) and dividing by the denominator, we observe the variable $\bar{r} = \frac{r}{R}$. The boundary conditions change (see Section 5).

$$\bar{P} = C\rho\omega R\left[a\phi\int_0^R \theta(\omega r)^2 - v_i(\omega r)dr + \int_0^R (\omega r)^2\, c_D dr\right] \tag{21}$$

$$c_P = \frac{\bar{P}}{\rho\pi R^2(\omega R)^3} = \frac{C\rho\omega R\left[a\phi\int_0^R \theta(\omega r)^2 - v_i(\omega r)dr + \int_0^R (\omega r)^2\, c_D dr\right]}{\rho\pi R^2(\omega R)^3}$$

$$c_P = \phi\int_0^1 \frac{Ca}{\pi R}\left(\theta\overline{r^2} - \phi\bar{r}\right)dr + \int_0^1 \frac{C}{\pi R}\left(\overline{r^3}c_D\right)dr$$

Notice, the first integral simplifies to the thrust coefficient (18). Solving the integral, we obtain the power coefficient (22).

$$c_P = \phi c_T + \int_0^1 \frac{C}{\pi R}\left(\overline{r^3}c_D\right)dr$$

$$c_P = \phi c_T + \frac{C}{4\pi R}c_D \tag{22}$$

The power coefficient can only be found after determining the drag coefficient.

### 6.1 Determining drag coefficient:

The drag coefficient incorporates resistive forces acting on a NACA 0015 aerofoil. Similar to the lift coefficient, drag coefficient is found using XFOIL. After inserting the calculated Reynolds numbers (Table 3), a $c_D$ vs α table is generated. Since, AoA is $\alpha = \theta - \phi = 0.157 - 0.0650 = 0.0920\ rad$, we select drag coefficients at $\alpha = 0.0920 rad$ for all angular velocities displayed in sample Table 5 to 3 sig.fig (see Appendix 5). Uncertainty is not calculated as XFOIL doesn't recognise error, decreasing confidence with drag coefficient.

**Table 5:** A table demonstrating drag coefficient ($c_D$) based on its constituent angular velocity ($\omega$).

| Angular velocity ($\omega$) | Tangential velocity ($\omega R$) | Reynolds Number ($Re$) | Lift curve gradient ($a$) | Drag coefficient ($c_D$) |
|---|---|---|---|---|
| $/rad\ s^{-1}$ | $/m\ s^{-1}$ | - | - | - |
| 0 | 0 | 0 | 0 | 0.0933 |
| 26 | 2.4 | $3\bar{0}00$ | 1.47 | 0.0756 |
| 50 | 5 | 6000 | 1.28 | 0.0683 |
| 79 | 7.1 | $9\bar{0}00$ | 1.23 | 0.0642 |
| 100 | 10 | 10000 | 1.22 | 0.0616 |
| ... | ... | ... | ... | ... |

### 6.2 Determining power coefficient:

We can now calculate power coefficient (22). Recall from section 5.3, in order to consider mechanical losses, we incorporate a constant $k = 1.75$.

$$c_P = k\left(\phi c_T + \frac{C}{4\pi R} c_D\right)$$

Substituting for the variables, we obtain power coefficient demonstrated in sample Table 7 (see Appendix 6). Uncertainty calculations are displayed bellow to 3 sig.fig, similar to the variable with lowest significant figure. However, we make an exception and increase significant figures of angular velocity to 3 sig.fig, for maximising accuracy and precision when analysing data.

| | |
|---|---|
| Fractional uncertainty for inflow AoA. | $\frac{\Delta\phi}{\phi} = \frac{0.00903}{0.0650} = 0.138 rad$ |
| Sum for the fractional uncertainties of $\phi$ and $c_T$ is that for $\phi c_T$. | $\frac{\Delta\phi c_T}{\phi c_T} = 0.138 + 0.684 = 0.822$ |
| Absolute uncertainty for $\phi c_T$ varies as $c_T$ changes with angular velocity. Example for $\omega = 26.2$ and rest shown in sample table 6. | $\phi c_T = 0.000233 \quad \Delta\phi c_T = 0.000233(0.822) = 0.000195$ |
| Fractional uncertainty for $\frac{C}{4\pi R} c_D$ is equivalent to that for $\frac{C}{R}$. | $\frac{\Delta\frac{C}{R}}{\frac{C}{R}} = 0.334$ from section 5.1. |

| | |
|---|---|
| Absolute uncertainty for $\frac{C}{4\pi R}c_D$ varies, as $c_D$ changes with angular velocity. Example for $\omega = 26.2$ and rest shown in sample table 6. | $\frac{C}{4\pi R}c_D = 0.00149 \quad \Delta\frac{C}{4\pi R}c_D = 0.00149(0.344) = 0.000496$ |
| Absolute uncertainty for $\phi c_T + \frac{C}{4\pi R}c_D$ (22) is sum of the absolute uncertainties for $\phi c_T$ and $\frac{C}{4\pi R}c_D$. Example for $\omega = 26.2$ and rest shown in sample table 6. | $\Delta\phi c_T + \frac{C}{4\pi R}c_D = 0.000195 + 0.000496 = 0.00691$ |
| Fractional uncertainty for $\phi c_T + \frac{C}{4\pi R}c_D$ is then allowed. Example for $\omega = 26.2$ and rest shown in sample table 6. | $\frac{\Delta\phi c_T + \frac{C}{4\pi R}c_D}{\phi c_T + \frac{C}{4\pi R}c_D} = \frac{0.00691}{0.00172} = 0.402$ |
| Fractional uncertainty for $\phi c_T + \frac{C}{4\pi R}c_D$ is equivalent to that for $c_P$. | $\frac{\Delta c_P}{c_P} = \frac{\Delta\phi c_T + \frac{C}{4\pi R}c_D}{\phi c_T + \frac{C}{4\pi R}c_D}$ |
| Absolute uncertainty for $c_P$ varies with $\omega$. Example for $\omega = 26.2$ and rest shown in sample table 7. | $c_P = 0.00301 \quad \Delta c_P = 0.00301(0.402) = 0.00121$ |

**Table 6:** Determining the absolute uncertainties of variables

| $\omega$ | $\phi c_T$ | $\Delta\phi c_T$ | $\frac{C}{4\pi R}c_D$ | $\Delta\frac{C}{4\pi R}c_D$ | $\phi c_T + \frac{C}{4\pi R}c_D$ | $\Delta\phi c_T + \frac{C}{4\pi R}c_D$ | $\frac{\Delta c_P}{c_P}$ |
|---|---|---|---|---|---|---|---|
| 26.2 | 0.000233 | 0.000195 | 0.00149 | 0.000496 | 0.00172 | 0.000691 | 0.402 |
| 52.4 | 0.000204 | 0.000170 | 0.00120 | 0.000402 | 0.00141 | 0.000572 | 0.407 |
| 78.5 | 0.000195 | 0.000164 | 0.00109 | 0.000363 | 0.00128 | 0.000526 | 0.411 |
| 104 | 0.000194 | 0.000162 | 0.00102 | 0.000341 | 0.00122 | 0.000504 | 0.414 |
| ... | ... | ... | ... | ... | ... | ... | ... |

**Table 7:** Determining the theoretical power coefficient and the coefficients absolute uncertainty

| **Angular velocity ($\omega$)** | **Power coefficient ($c_P$)** | **Absolute uncertainty $\Delta c_P$** |
|---|---|---|
| $rads^{-1}$ | - | - |
| 0 | 0 | 0 |
| 26.2 | 0.00301 | 0.00121 |
| 52.4 | 0.00246 | 0.00100 |
| 78.5 | 0.00224 | 0.000921 |
| 104 | 0.00213 | 0.000881 |
| ... | ... | ... |

The data in Table 7 is represented as a graph in Figure 11. For a system to be power efficient, the thrust and power to area ratio must strictly maximise and minimise respectively. The mean of all power coefficient data points are represented as a mean line. The angular velocities between $0 - 183rads^{-1}$ are power inefficient, as they demonstrate a low thrust (see Figure 9), but a large power coefficient. This suggests most power is used to overcome resistive forces. Moreover, angular velocities between $183 - 733rads^{-1}$ in retrospect are not power efficient, as they have a large thrust and power coefficient. Here, most power is used to generate thrust than lost to air resistance and therefore, has ideal efficiency contrary to speculations.

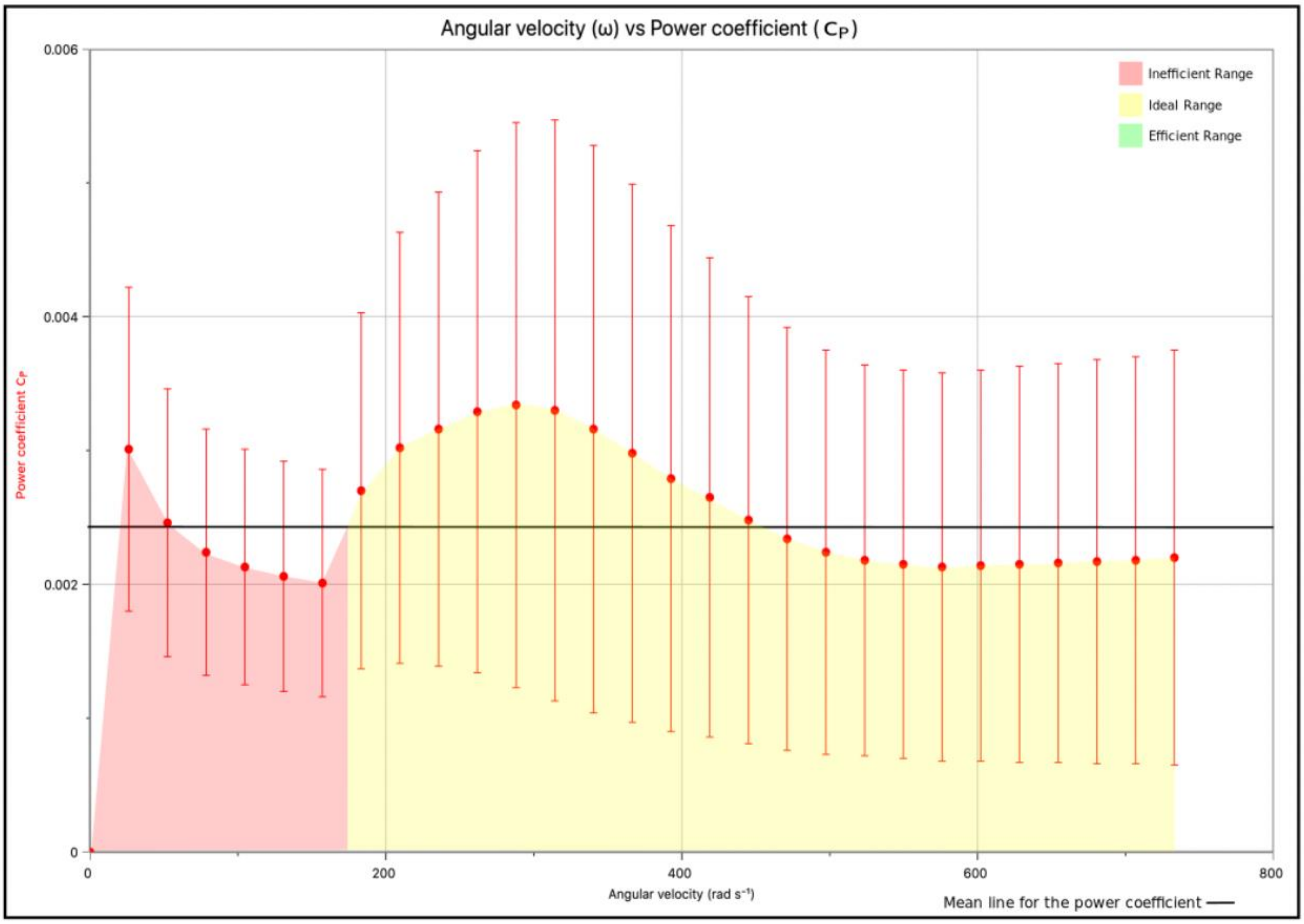


**Figure 11:** The relationship between angular velocity and power coefficient

## 7.0 Determining Experimental Power Coefficient

An experiment was designed to observe power dissipated, later converted to power coefficient in revolving a twin bladed airscrew by a brushless DC motor (BLDC motor). Thrust measurements for determining thrust coefficient are not accounted, as the measuring scale provided misleading results (see Figure 12). The experiment is necessary to validate whether the theoretical data (see section 5.3 and 6.2) corresponds with experimental data. This is important as it allows to find a reason for the large error bars seen with the coefficients, any sources of error or confounding variables.

### 7.1 Experimental Setup

In 1920-33, the National Advisory Committee for Aeronautics (NACA) designed and tested various standardised aerofoils (Allen, 2017). I selected their NACA 0015 aerofoil, for its symmetric geometry and ease to 3D print. The aerofoil was printed with dimensions stated in Table 8 and went on top of BLDC motor.

**Table 8:** A description for the properties of NACA 0015 aerofoil

| Aerofoil Geometry | Properties |
|---|---|
| NACA 0015 | Blade length: Radius $R = 0.0900 \pm 0.00500m$<br>Blade length: Chord width $C = 0.0180 \pm 0.00500m$<br>Total angle: Pitch angle $\theta = 0.157 \pm 0.00900rad$ |

The experiment setup is represented in Figure 12. An Arduino Mega 2560 microcontroller used a preloaded code (see Appendix 9) to change RPM of motor (Nedelkovski, 2019). A tachometer measures the frequency of reflections from a reflective adhesive on the motor to determine the motors RPM. A power analyser measured the total power used by the load. A camera positioned above the setup, recorded the displayed readings.

### 7.2 Experiment procedure

- **Independent variable:** Angular velocity measured in RPM.
- **Dependent variable:** Power dissipated in the system.

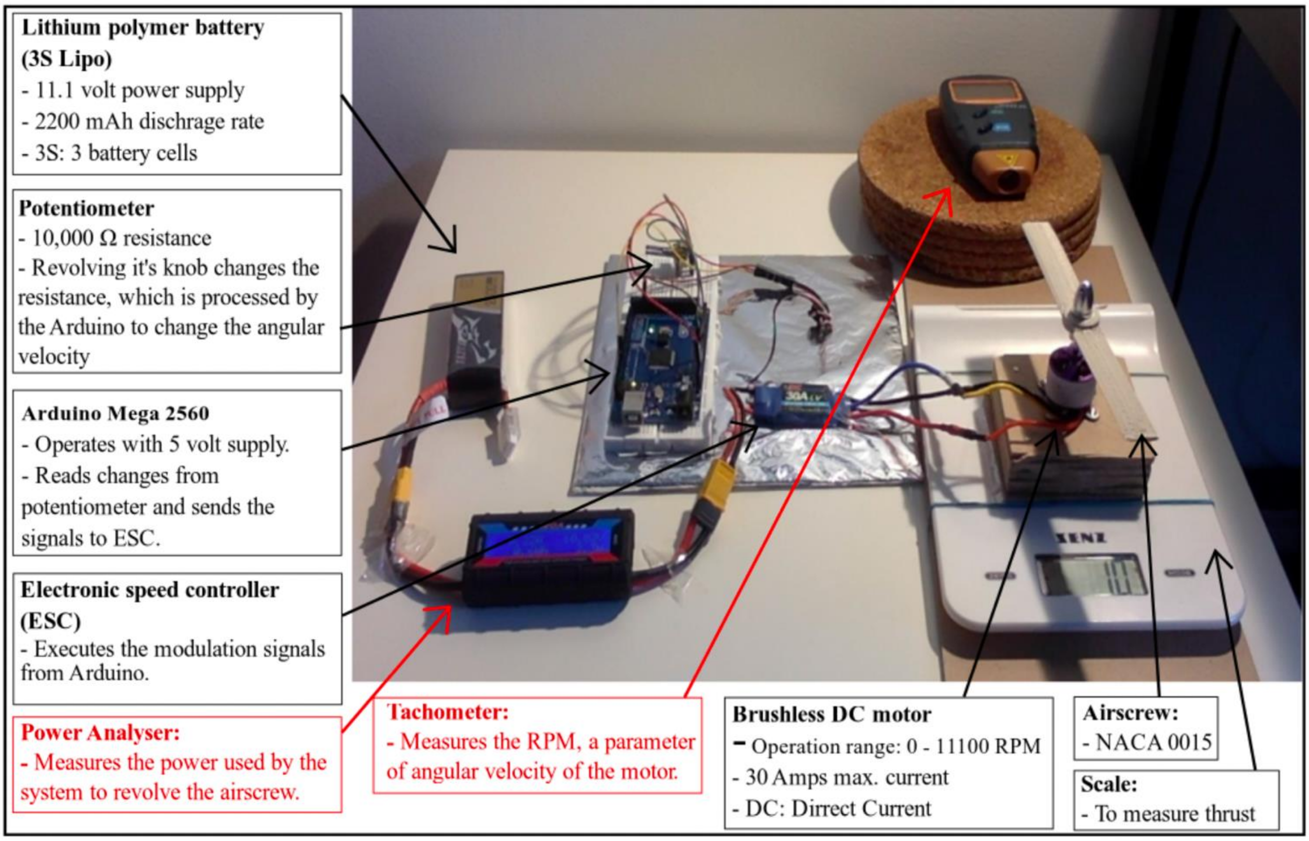


**Figure 12:** The experimental setup for determining the power coefficient.

A physical limitation of the motor is, it harshly vibrated between $0 < \omega \leq 314rads^{-1}$ and $681 \leq \omega < 733rads^{-1}$ deviating the photo tachometer readings. I realised to minimise systematic error; the testing range should be between $314 \leq \omega \leq 681rads^{-1}$. Additionally, the angular velocity readings never remained constant while performing preliminary tests. Hence, I decided the experiment would be conducted in intervals of $250\ RPM$ ($26.2rads^{-1}$) beginning from $301 < \omega \leq 327rads^{-1}$ and ending with $668 < \omega \leq 694 rads^{-1}$. Each interval would be tested 5 times, for 15 seconds with a stopwatch. The data was collected from video recordings and is displayed in Appendix 7.

### 7.2 Theoretical vs experimental power coefficient

The RPM were converted to angular velocity using the factor $\frac{2\pi}{60}$ (see Section 5.2). The angular velocity within an interval is best demonstrated by its mean. The mean for power measured within the interval, is suitable for the same reasoning. Such means are demonstrated in sample Table 9 for the first 5 intervals. Recall, the power coefficient (9). Substituting values from Table 9 yields the experimental power coefficient, also shown in sample Table 9.

$$c_P = \frac{\bar{P}}{\rho\pi R^2(\bar{\omega}R)^3}$$

**Table 9:** Determining the experimental power coefficient.

| Angular velocity | Mean angular velocity ($\bar{\omega}$) | Mean power ($\bar{P_{avg}}$) | Experimental power coefficient ($c_P$) |
|---|---|---|---|
| $rads^{-1}$ | $rads^{-1}$ | $kgm^2s^{-3}$ | - |
| $301 < \omega \leq 327$ | 318 | 2.8 | 0.00389 |
| $327 < \omega \leq 353$ | 343 | 3.4 | 0.00363 |
| $353 < \omega \leq 380$ | 367 | 3.7 | 0.00326 |
| $380 < \omega \leq 406$ | 397 | 4.3 | 0.00302 |
| $406 < \omega \leq 432$ | 420 | 4.9 | 0.00290 |
| ... | ... | ... | ... |

The experimental and theoretical data points from Table 7 and 9 are illustrated as a graph in Figure 13, with ordinates drawn to indicate the experimented range. Both curves are close to perfect fit, as the experimental outcomes are more exaggerated deviating around 314 and 680 $rads^{-1}$. Nevertheless, both power coefficients have similar properties such as, a curve fit which monotonically decreases with angular velocity. Their gradient ($\frac{dc_P}{d\omega}$) converges to 0 from 550 to 600 $rads^{-1}$ as both curves either seem to or form a plateau. Error bars are also useful, as experimental data follows the trend well within the error bars of the theoretical data. Hence, the theoretical model closely resembles outcomes from the experiment.

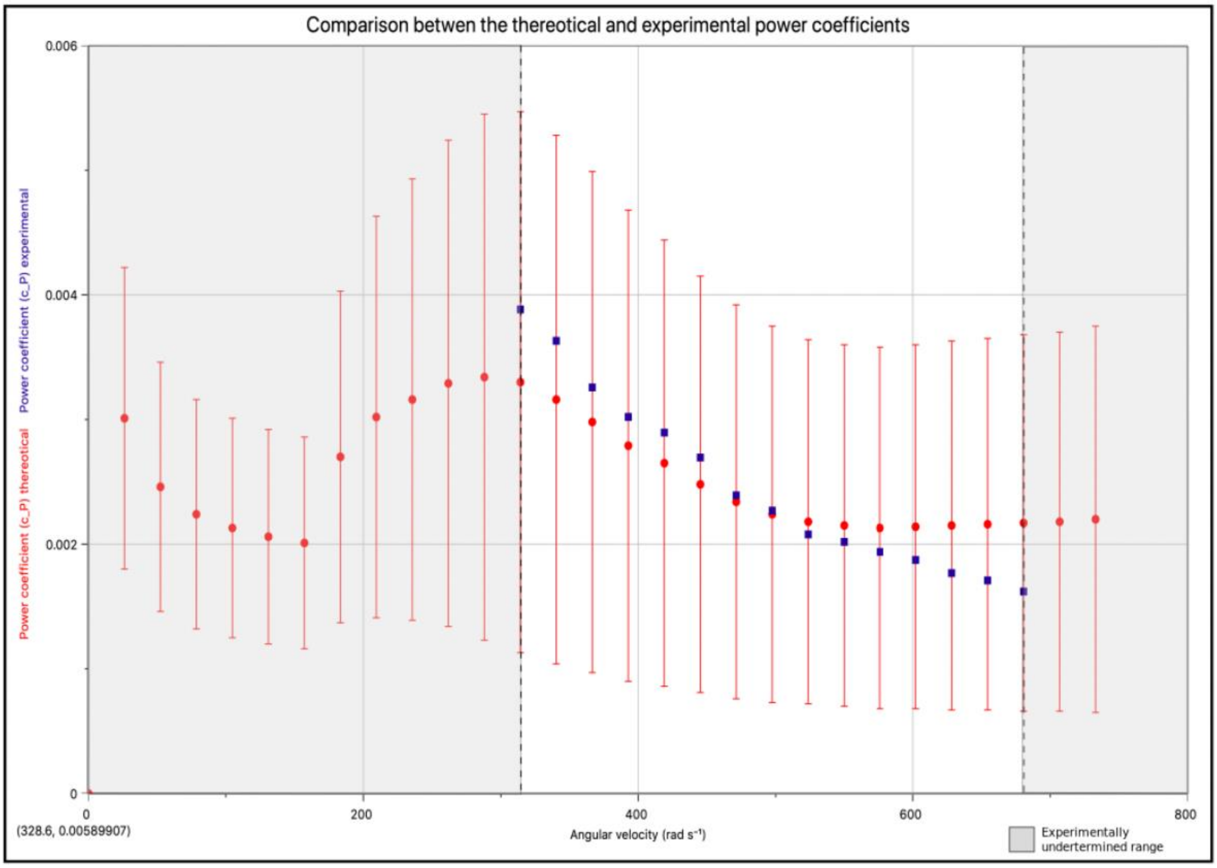


**Figure 13:** An analysis between angular velocity and power coefficient

## 8.0 Determining Power Efficiency

Realise, we can finally determine power efficiency (11). Substituting the trust and power coefficient, yields power efficiency displayed in sample Table 10 (see Appendix 8).

$$\eta = 70.7 \times \frac{c_T^{\frac{3}{2}}}{c_P}$$

Uncertainty for power efficiency is propagated with steps displayed below.

| | |
|---|---|
| Fractional uncertainty for numerator $c_T^{\frac{3}{2}}$. | $\frac{\Delta c_T^{\frac{3}{2}}}{c_T^{\frac{3}{2}}} = \frac{3}{2}(\frac{\Delta c_T}{c_T}) = 1.50(0.684) = 1.09$ |
| Fractional uncertainty for denominator $c_P$ is demonstrated in table 6 | |
| Fractional uncertainty for power efficiency ($\eta$) is sum of the fractional uncertainties for numerator $c_T^{\frac{3}{2}}$ and denominator $c_P$. An example is $\omega = 26.2rads^{-1}$ and rest are shown in table 10. | $\frac{\Delta\eta}{\eta} = \frac{\Delta c_T^{\frac{3}{2}}}{c_T^{\frac{3}{2}}} + \frac{\Delta c_P}{c_P} = 1.09 + 0.00301 = 1.49$ |
| The absolute uncertainty for power efficiency can then be found. An example is $\omega = 26.2rads^{-1}$ and rest are shown in table 10. | $\eta = 5.05 \quad \Delta\eta = 5.05(1.49) = 7.54$ |

**Table 10:** Calculations for determining the power efficiency of our twin bladed single rotor helicopter system.

| Angular velocity ($\omega$) | Power efficiency ($\eta$) | Fractional uncertainty ($\frac{\Delta\eta}{\eta}$) | Absolute uncertainty ($\Delta\eta$) |
|---|---|---|---|
| $rads^{-1}$ | $kgm^2s^{-3}$ | - | $kgm^2s^{-3}$ |
| 26.2 | 5.05 | 1.49 | 7.54 |
| 52.4 | 5.04 | 1.50 | 7.54 |
| 78.5 | 5.20 | 1.50 | 7.80 |
| 105 | 5.42 | 1.50 | 8.15 |
| ... | ... | ... | ... |

Table 10 is then converted to a power efficiency against angular velocity graph in Figure 14. The general trend line increases and plateaus in a regular succession. Power efficiency at smaller angular velocities ($0 - 157rads^{-1}$) are an order of magnitude inefficient than at larger ones ($314 - 733rads^{-1}$) confirming the inefficient and ideal ranges respectively. The maximum efficiency peaks at 54.6% is just under the maximum possible efficiency by Betz limit at 59.3% (Burton, 2009). Negative uncertainties cannot exist. As aforementioned, large uncertainties are caused by exhaustively using multiple equations to reach this relationship. Hence, the data quality is not compromised.

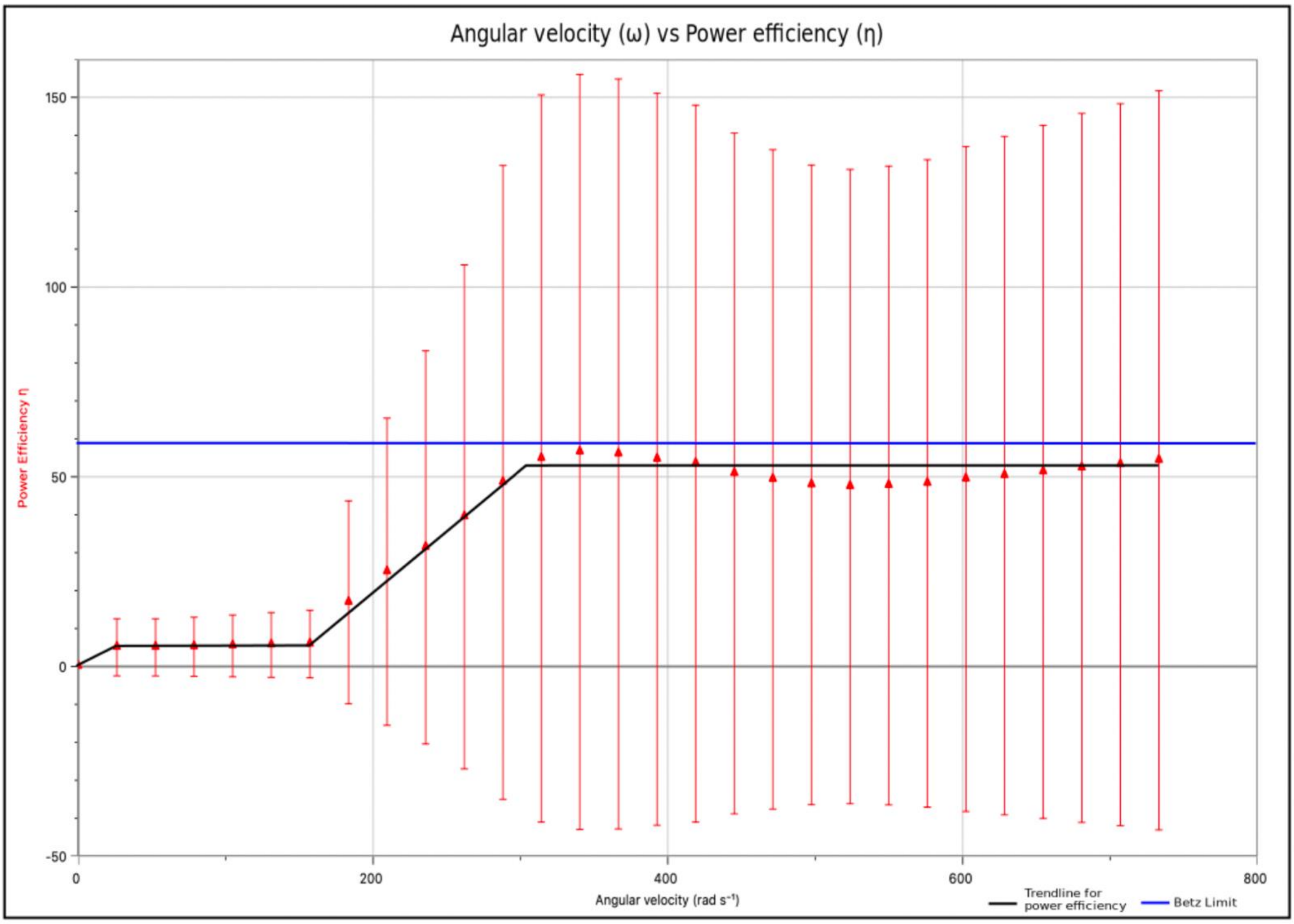


**Figure 14:** The relationship between power efficiency and angular velocity.

## 9.0 Evaluation and Conclusion

In investigating the research question, we decided to determine power efficiency with the thrust and power coefficient, resulting in many interesting observations.

Firstly, we found a limitation with Froude's model, in that it assumed a zero-pitch system, omitting internal forces and velocities. Hence, modifications such as blade element theory were made to implement pitch, enhancing the correlation between empirical and theoretical data.

In determining the thrust coefficient, XFOIL allowed to find lift-curve gradient and an analysis with industrial specification. This categorised angular velocity into an inefficient, ideal and efficient range, where smaller angular velocities in comparison to larger angular velocities required a substantial amount of power to overcome resistive forces. The power coefficient showed similar efficiencies, except for the efficient range. The experiment validated the theoretical ranges and realised the large uncertainties were of a purely mathematical consequence. Hence, the inefficient and ideal ranges were confirmed as maximum power efficiency peaked only at 54.6%. However, a limitation with this experiment was the small, experimented range for angular velocity, not allowing a full comparison with the theoretical model.

In conclusion a clear proportionality is visible between angular velocity and power efficiency for a twin bladed single rotor helicopter in hover. As we increase angular velocity, power efficiency increases then plateaus and repeats the same trend once again.

This investigation is not completely accurate, due to uncertainties and limitations. A part of these uncertainties arises from assumptions made within the theoretical model. For instance, assuming thrust linearly increases along the blade. Empirically, the tip produces negligible thrust, as the substantial dynamic pressure differential occurs from 20 to 80% of the blade (Adminstration, 2020). Secondly, a vortex known as induced drag is formed at the blade's tip, which moderately increases air resistance. This was not implemented in XFOIL adding unaccounted systematic error (Adminstration, 2020). Thirdly, the motor harshly vibrated at the first ($301 < \omega \leq 327 rads^{-1}$) and last interval ($668 < \omega \leq 694 rads^{-1}$), influencing the tachometer and power analyser, causing random error in data. This may explain deviations at the start and end of the experimental power coefficient. However, I realised that seeking for a perfect match with the experimental data is ambitious, as the investigation then becomes an extraneous mathematical process reducing its ability to explain physics.

This investigation raises many questions, including one which initially inspired me: what angular velocity against power efficiency relationship can geometrically varied aerial vehicles such as, bicopters and tricopters demonstrate? Irregularly positioning rotor systems, makes the slipstream geometry unique and transcends the scope of this investigation. Many interesting problems arise, as the rotors must produce variable thrust to balance while hovering. Such an investigation would be incredibly interesting.

## 10.0 Works Cited


Administration, F. (2020). *Rotorcraft Flying Handbook* (pp. 2-28). BN Publishing.

Allen, B. (2017). *NACA Airfoils*. National Aeronautics and Space Administration. Retrieved 24 December 2020, from https://www.nasa.gov/image-feature/langley/100/naca-airfoils.

Burton, T. (2009). *Wind energy* (1st ed., p. 6). Wiley.
Gessow, A., & Myers, G. (1985). *Aerodynamics of the helicopter* (8th ed., pp. 46-65).

Ungar.

Halliday, D., Resnick, R., Walker, J., & Halliday, D. (2014). *Fundamentals of physics* (11th ed., pp. 386-412). Wiley.

*Helicopter Career Info*. Heliventures.co. (2017). Retrieved 4 September 2020, from https://www.heliventures.co/new-helicopter-pilot-resources/helicopter-career-info/.

Lombardi, F. (2017). *Understanding Helicopter Power Requirements: The Power Struggle - Rotor & Wing International*. Rotor & Wing International. Retrieved 25 December 2020, from https://www.rotorandwing.com/2017/10/10/understanding-helicopter-power-require ments-power-struggle/.

Nedelkovski, D. (2019). *Arduino Brushless Motor Control Tutorial*. HowToMechatronics. Retrieved 26 June 2020, from https://howtomechatronics.com/tutorials/arduino/arduino-brushless-motor-control-tu torial-esc-bldc/.

Scott, J. (2018). *Lift Coefficient & Thin Airfoil Theory*. Aerospaceweb. Retrieved 28 November 2020, from http://www.aerospaceweb.org/question/aerodynamics/q0136.shtml#:~:text=Accordi ng%20to%20the%20ideal%20aerodynamics,%CE%B1)%20is%20equal%20to%20 2%CF%80.&text=According%20to%20Thin%20Airfoil%20Theory,(CL)%20goes %20up.

Venkatesan. (2012). *Hovering Theory:Blade Element Theory*. Lecture, Indian Institute of Technology Kanpur.

Zhao, D., Han, N., Goh, E., Cater, J., & Reinecke, A. (2019). *Wind turbines and aerodynamics energy harvesters* (pp. 1-5). Elsevier.

# Appendix 1: Simplifying Reynolds Number

Reynolds number measures airflow patterns, based on the properties of air. In fluid mechanics one form Reynolds number can take is displayed bellow. Here, $\nu$ is kinematic viscosity, $v_r$ is resultant velocity of airfoil and $C$ is chord length. Kinematic viscosity of air at sea level and normal room temperature is: $\nu = 1.42 \times 10^{-5}$.

$$Re = \frac{Cv}{\nu}$$

We substitute the value for variables from section 7 and use resultant velocity (15). However, realise $v_R = \omega r \approx \omega R$ as dynamic pressure is substantially large at the tip and approximately equal to that across the blade. Hence, by venturi effect tangential velocity at tip is also approximately equal to that across the blade.

$$Re = \frac{(0.0180)\omega R}{0.0000142}$$

$$Re = 1266.98\omega R$$

# Appendix 2: Conversion between Angular Velocity and Reynolds Number

| Revolution per minute (RPM) | Angular velocity (ω) | Tangential velocity (ωR) | Reynolds Number (Re) |
|---|---|---|---|
| $/min^{-1}$ | $/rads^{-1}$ | $/ms^{-1}$ | - |
| 0 | 0 | 0.0 | 0 |
| 250 | 26 | 2.4 | 2991 |
| 500 | 52 | 4.7 | 5982 |
| 750 | 79 | 7.1 | 8972 |
| 1000 | 105 | 9.4 | 11963 |
| 1250 | 131 | 11.8 | 14954 |
| 1500 | 157 | 14.1 | 17945 |
| 1750 | 183 | 16.5 | 20935 |
| 2000 | 209 | 18.8 | 23926 |
| 2250 | 236 | 21.2 | 26917 |
| 2500 | 262 | 23.6 | 29908 |
| 2750 | 288 | 25.9 | 32899 |
| 3000 | 314 | 28.3 | 35889 |
| 3250 | 340 | 30.6 | 38880 |
| 3500 | 367 | 33.0 | 41871 |
| 3750 | 393 | 35.3 | 44862 |
| 4000 | 419 | 37.7 | 47853 |
| 4250 | 445 | 40.1 | 50843 |
| 4500 | 471 | 42.4 | 53834 |
| 4750 | 497 | 44.8 | 56825 |
| 5000 | 524 | 47.1 | 59816 |
| 5250 | 550 | 49.5 | 62806 |
| 5500 | 576 | 51.8 | 65797 |
| 5750 | 602 | 54.2 | 68788 |
| 6000 | 628 | 56.5 | 71779 |
| 6250 | 654 | 58.9 | 74770 |
| 6500 | 681 | 61.3 | 77760 |
| 6750 | 707 | 63.6 | 80751 |
| 7000 | 733 | 66.0 | 83742 |

## Appendix 3: Determination of Lift-curve Gradient

| Angular velocity (ω) | Tangential velocity (ωR) | Reynolds Number (Re) | Lift-curve gradient (a) |
|---|---|---|---|
| $/rads^{-1}$ | $/ms^{-1}$ | - | - |
| 0 | 0.0 | 0 | 0.00 |
| 26 | 2.4 | 2991 | 1.47 |
| 52 | 4.7 | 5982 | 1.28 |
| 79 | 7.1 | 8972 | 1.23 |
| 105 | 9.4 | 11963 | 1.22 |
| 131 | 11.8 | 14954 | 1.23 |
| 157 | 14.1 | 17945 | 1.25 |
| 183 | 16.5 | 20935 | 3.06 |
| 209 | 18.8 | 23926 | 4.28 |
| 236 | 21.2 | 26917 | 5.14 |
| 262 | 23.6 | 29908 | 6.14 |
| 288 | 25.9 | 32899 | 7.13 |
| 314 | 28.3 | 35889 | 7.66 |
| 340 | 30.6 | 38880 | 7.60 |
| 367 | 33.0 | 41871 | 7.26 |
| 393 | 35.3 | 44862 | 6.84 |
| 419 | 37.7 | 47853 | 6.51 |
| 445 | 40.1 | 50843 | 6.02 |
| 471 | 42.4 | 53834 | 5.69 |
| 497 | 44.8 | 56825 | 5.42 |
| 524 | 47.1 | 59816 | 5.27 |
| 550 | 49.5 | 62806 | 5.25 |
| 576 | 51.8 | 65797 | 5.26 |
| 602 | 54.2 | 68788 | 5.36 |
| 628 | 56.5 | 71779 | 5.44 |
| 654 | 58.9 | 74770 | 5.52 |
| 681 | 61.3 | 77760 | 5.62 |
| 707 | 63.6 | 80751 | 5.70 |

## Appendix 4: Determination of Thrust Coefficient

| Air screw geometry $(R, C)$ | Aircrew Angles $(\theta, \phi)$ | Angular velocity (ω) | Gradient of lift-curve (a) | Thrust Coefficient ($c_T$) |
|---|---|---|---|---|
| $/m$ | $/rad$ | $/rads^{-1}$ | - | - |
| **± 0.00500, ±0.00500** | **±0.00900, ±0.00900** | **-** | **-** | **68.40%** |
| 0.0900, 0.0180 | 0.157, 0.0650 | 0 | 0.00 | 0.00000 |
| | | 26 | 1.47 | 0.00359 |
| | | 52 | 1.28 | 0.00313 |
| | | 79 | 1.23 | 0.00301 |
| | | 105 | 1.22 | 0.00299 |
| | | 131 | 1.23 | 0.00301 |
| | | 157 | 1.25 | 0.00305 |
| | | 183 | 3.06 | 0.00747 |
| | | 209 | 4.28 | 0.01044 |
| | | 236 | 5.14 | 0.01253 |
| | | 262 | 6.14 | 0.01497 |
| | | 288 | 7.13 | 0.01738 |
| | | 314 | 7.66 | 0.01870 |
| | | 340 | 7.60 | 0.01854 |
| | | 367 | 7.26 | 0.01772 |
| | | 393 | 6.84 | 0.01670 |
| | | 419 | 6.51 | 0.01588 |
| | | 445 | 6.02 | 0.01470 |
| | | 471 | 5.69 | 0.01387 |
| | | 497 | 5.42 | 0.01321 |
| | | 524 | 5.27 | 0.01287 |
| | | 550 | 5.25 | 0.01281 |
| | | 576 | 5.26 | 0.01284 |
| | | 602 | 5.36 | 0.01308 |
| | | 628 | 5.44 | 0.01327 |
| | | 654 | 5.52 | 0.01347 |
| | | 681 | 5.62 | 0.01371 |
| | | 707 | 5.70 | 0.01391 |
| | | 733 | 5.82 | 0.01420 |

# Appendix 5: Determination of Drag Coefficient

| Angular velocity (ω) | Tangential velocity (ωR) | Reynolds Number (Re) | Lift-curve gradient (a) | Drag coefficient ($c_D$) |
|---|---|---|---|---|
| $/rads^{-1}$ | $/ms^{-1}$ | - | - | - |
| 0 | 0.0 | 0 | 0.00 | 0.0000 |
| 26 | 2.4 | 2991 | 1.47 | 0.0933 |
| 52 | 4.7 | 5982 | 1.28 | 0.0756 |
| 79 | 7.1 | 8972 | 1.23 | 0.0683 |
| 105 | 9.4 | 11963 | 1.22 | 0.0642 |
| 131 | 11.8 | 14954 | 1.23 | 0.0616 |
| 157 | 14.1 | 17945 | 1.25 | 0.0598 |
| 183 | 16.5 | 20935 | 3.06 | 0.0664 |
| 209 | 18.8 | 23926 | 4.28 | 0.0658 |
| 236 | 21.2 | 26917 | 5.14 | 0.0623 |
| 262 | 23.6 | 29908 | 6.14 | 0.0568 |
| 288 | 25.9 | 32899 | 7.13 | 0.0490 |
| 314 | 28.3 | 35889 | 7.66 | 0.0421 |
| 340 | 30.6 | 38880 | 7.60 | 0.0376 |
| 367 | 33.0 | 41871 | 7.26 | 0.0345 |
| 393 | 35.3 | 44862 | 6.84 | 0.0321 |
| 419 | 37.7 | 47853 | 6.51 | 0.0302 |
| 445 | 40.1 | 50843 | 6.02 | 0.0289 |
| 471 | 42.4 | 53834 | 5.69 | 0.0275 |
| 497 | 44.8 | 56825 | 5.42 | 0.0266 |
| 524 | 47.1 | 59816 | 5.27 | 0.0256 |
| 550 | 49.5 | 62806 | 5.25 | 0.0249 |
| 576 | 51.8 | 65797 | 5.26 | 0.0241 |
| 602 | 54.2 | 68788 | 5.36 | 0.0235 |
| 628 | 56.5 | 71779 | 5.44 | 0.0229 |
| 654 | 58.9 | 74770 | 5.52 | 0.0224 |
| 681 | 61.3 | 77760 | 5.62 | 0.0219 |
| 707 | 63.6 | 80751 | 5.70 | 0.0215 |

# Appendix 6: Determination of Power Coefficient

| Angular velocity (ω) | Power coefficient ($c_P$) | Absolute uncertainty $\Delta c_P$ |
|---|---|---|
| $/rads^{-1}$ | - | - |
| 0 | 0 | 0 |
| 26 | 0.00172 | 0.001209 |
| 52 | 0.00141 | 0.001001 |
| 79 | 0.00128 | 0.000921 |
| 105 | 0.00122 | 0.000881 |
| 131 | 0.00118 | 0.000860 |
| 157 | 0.00115 | 0.000847 |
| 183 | 0.00154 | 0.001328 |
| 209 | 0.00173 | 0.001605 |
| 236 | 0.00181 | 0.001772 |
| 262 | 0.00188 | 0.001954 |
| 288 | 0.00191 | 0.002111 |
| 314 | 0.00188 | 0.002172 |
| 340 | 0.00180 | 0.002116 |
| 367 | 0.00170 | 0.002008 |
| 393 | 0.00160 | 0.001889 |
| 419 | 0.00151 | 0.001793 |
| 445 | 0.00142 | 0.001668 |
| 471 | 0.00134 | 0.001576 |
| 497 | 0.00128 | 0.001505 |
| 524 | 0.00124 | 0.001463 |
| 550 | 0.00123 | 0.001451 |
| 576 | 0.00122 | 0.001447 |
| 602 | 0.00122 | 0.001464 |
| 628 | 0.00123 | 0.001476 |
| 654 | 0.00123 | 0.001491 |
| 681 | 0.00124 | 0.001510 |
| 707 | 0.00125 | 0.001524 |

## Appendix 7: Raw Experimental Data

| # | 2875 < rpm ≤ 3125 | Power | 3125 < rpm ≤ 3375 | Power | 3375 < rpm ≤ 3625 | Power | 3625 < rpm ≤ 3875 | Power |
|---|---|---|---|---|---|---|---|---|
| 1 | 3017 | 2.9 | 3267 | 3.2 | 3417 | 3.3 | 3736 | 4.2 |
| 2 | 3017 | 3.1 | 3269 | 3.3 | 3434 | 3.5 | 3737 | 4.3 |
| 3 | 3018 | 3.0 | 3269 | 3.3 | 3436 | 3.1 | 3738 | 4.4 |
| 4 | 3019 | 3.3 | 3270 | 3.3 | 3445 | 3.5 | 3739 | 4.2 |
| 5 | 3020 | 3.1 | 3271 | 3.4 | 3447 | 3.8 | 3740 | 4.3 |
| 6 | 3022 | 2.7 | 3271 | 3.3 | 3450 | 3.8 | 3740 | 4.3 |
| 7 | 3022 | 2.8 | 3272 | 3.4 | 3453 | 3.5 | 3742 | 4.4 |
| 8 | 3023 | 2.9 | 3272 | 3.4 | 3453 | 3.7 | 3742 | 4.3 |
| 9 | 3029 | 2.8 | 3272 | 3.3 | 3459 | 3.7 | 3743 | 4.3 |
| 10 | 3030 | 2.8 | 3273 | 3.1 | 3460 | 3.7 | 3753 | 4.2 |
| 11 | 3039 | 3.2 | 3275 | 3.4 | 3461 | 3.6 | 3758 | 4.3 |
| 12 | 3040 | 3.2 | 3276 | 3.4 | 3462 | 3.8 | 3759 | 4.1 |
| 13 | 3042 | 2.4 | 3277 | 3.4 | 3464 | 3.6 | 3760 | 4.3 |
| 14 | 3042 | 3.0 | 3278 | 3.3 | 3472 | 3.3 | 3761 | 4.2 |
| 15 | 3043 | 2.7 | 3282 | 3.3 | 3474 | 3.8 | 3761 | 4.2 |
| 16 | 3043 | 2.7 | 3292 | 3.6 | 3478 | 4.0 | 3761 | 4.2 |
| 17 | 3044 | 2.4 | 3296 | 3.4 | 3496 | 3.8 | 3762 | 4.2 |
| 18 | 3044 | 2.8 | 3298 | 3.3 | 3500 | 3.3 | 3764 | 4.4 |
| 19 | 3044 | 2.6 | 3298 | 3.6 | 3516 | 3.7 | 3765 | 4.2 |
| 20 | 3045 | 2.4 | 3299 | 3.4 | 3517 | 3.4 | 3765 | 4.2 |
| 21 | 3045 | 2.8 | 3300 | 3.4 | 3518 | 3.8 | 3766 | 4.3 |
| 22 | - |  | - | - | 3536 | 3.6 | 3767 | 4.2 |
| 23 | - | - | - | - | 3538 | 3.6 | 3768 | 4.3 |
| 24 | - | - | - | - | 3540 | 3.8 | 3773 | 4.4 |
| 25 | - | - | - | - | 3541 | 3.8 | 3851 | 4.5 |
| 26 | - | - | - | - | 3546 | 3.8 | 3854 | 4.3 |
| 27 | - | - | - | - | 3547 | 3.7 | 3855 | 4.3 |
| 28 | - | - | - | - | 3548 | 3.7 | 3855 | 4.4 |
| 29 | - | - | - | - | 3548 | 3.7 | 3856 | 4.4 |
| 30 | - | - | - | - | 3548 | 3.8 | 3857 | 4.4 |
| 31 | - | - | - | - | 3549 | 3.8 | 3863 | 4.4 |
| 32 | - | - | - | - | 3549 | 3.9 | 3864 | 4.4 |
| 33 | - | - | - | - | 3550 | 3.8 | 3866 | 4.4 |
| 34 | - | - | - | - | 3552 | 3.8 | 3867 | 4.4 |
| 35 | - | - | - | - | 3553 | 3.6 | 3867 | 4.4 |
| 36 | - | - | - | - | 3556 | 3.8 | 3875 | 4.4 |
| 37 | - | - | - | - | 3559 | 3.8 | - | - |
| 38 | - | - | - | - | 3567 | 3.8 | - | - |
| 39 | - | - | - | - | 3575 | 3.9 | - | - |

| # | 3875 < rpm ≤ 4125 | Power | 4125 < rpm ≤ 4375 | Power | 4375 < rpm ≤ 4625 | Power | 4625 < rpm ≤ 4875 | Power |
|---|---|---|---|---|---|---|---|---|
| 1 | 3964 | 4.9 | 4141 | 5.5 | 4478 | 5.6 | 4699 | 6.4 |
| 2 | 3965 | 4.9 | 4157 | 5.2 | 4479 | 5.7 | 4705 | 6.5 |
| 3 | 3966 | 4.8 | 4161 | 5.3 | 4482 | 5.6 | 4708 | 6.2 |
| 4 | 3971 | 4.9 | 4165 | 5.4 | 4484 | 5.7 | 4708 | 6.2 |
| 5 | 3973 | 5.2 | 4165 | 5.4 | 4485 | 5.8 | 4709 | 6.4 |
| 6 | 3973 | 4.9 | 4167 | 5.2 | 4485 | 5.6 | 4710 | 6.5 |
| 7 | 3974 | 4.9 | 4167 | 5.5 | 4486 | 5.6 | 4711 | 6.5 |
| 8 | 3974 | 4.9 | 4169 | 5.2 | 4486 | 5.5 | 4712 | 6.4 |
| 9 | 3975 | 4.9 | 4169 | 5.3 | 4488 | 5.6 | 4712 | 6.5 |
| 10 | 3975 | 5.1 | 4259 | 5.3 | 4488 | 5.5 | 4713 | 6.0 |
| 11 | 3975 | 5.1 | 4261 | 5.1 | 4489 | 5.5 | 4713 | 6.5 |
| 12 | 3977 | 4.7 | 4262 | 4.9 | 4489 | 5.7 | 4714 | 6.5 |
| 13 | 3977 | 4.8 | 4263 | 5.5 | 4490 | 5.6 | 4714 | 6.0 |
| 14 | 3978 | 4.9 | 4263 | 5.5 | 4494 | 5.6 | 4715 | 6.2 |
| 15 | 3978 | 4.8 | 4263 | 5.4 | 4535 | 6.3 | 4716 | 6.5 |
| 16 | 3978 | 4.8 | 4264 | 5.4 | 4537 | 6.0 | 4716 | 6.4 |
| 17 | 3979 | 4.9 | 4264 | 5.5 | 4539 | 6.3 | 4717 | 6.5 |
| 18 | 3980 | 4.9 | 4264 | 5.5 | 4541 | 6.0 | 4719 | 6.6 |
| 19 | 3980 | 4.9 | 4264 | 5.3 | 4541 | 5.7 | 4719 | 6.5 |
| 20 | 3981 | 5.1 | 4264 | 5.3 | 4546 | 6.0 | 4720 | 6.0 |
| 21 | 3981 | 4.7 | 4265 | 5.4 | 4547 | 5.9 | 4720 | 6.4 |
| 22 | 3981 | 5.0 | 4265 | 5.2 | 4547 | 5.8 | 4721 | 6.5 |
| 23 | 3983 | 4.8 | 4265 | 5.2 | 4548 | 6.3 | 4723 | 6.0 |
| 24 | 3984 | 4.8 | 4266 | 5.5 | 4549 | 6.3 | 4724 | 5.9 |
| 25 | 3984 | 4.8 | 4266 | 5.6 | 4550 | 6.1 | 4725 | 6.2 |
| 26 | 4024 | 4.8 | 4266 | 5.4 | 4551 | 6.3 | 4726 | 6.0 |
| 27 | 4031 | 4.9 | 4266 | 5.5 | 4551 | 5.9 | 4728 | 6.0 |
| 28 | 4032 | 4.9 | 4267 | 5.6 | 4552 | 6.0 | 4729 | 6.0 |
| 29 | 4037 | 4.8 | 4267 | 5.8 | 4552 | 5.8 | 4731 | 6.1 |
| 30 | 4038 | 4.9 | 4267 | 5.4 | 4554 | 6.0 | 4732 | 6.4 |
| 31 | 4038 | 4.9 | 4269 | 5.2 | 4555 | 6.3 | 4732 | 6.5 |
| 32 | 4043 | 4.8 | 4270 | 5.7 | 4555 | 5.9 | 4734 | 6.0 |
| 33 | 4044 | 4.9 | 4271 | 5.6 | 4556 | 6.0 | 4735 | 6.2 |
| 34 | 4045 | 4.8 | 4271 | 5.5 | 4556 | 5.9 | 4862 | 6.6 |
| 35 | 4045 | 5.1 | 4271 | 5.2 | 4557 | 5.9 | 4864 | 6.8 |
| 36 | 4047 | 4.8 | 4274 | 5.3 | 4557 | 5.9 | 4866 | 6.6 |
| 37 | 4047 | 4.9 | - | - | 4558 | 6.0 | 4872 | 6.8 |
| 38 | 4048 | 5.0 | - | - | 4558 | 5.9 | 4873 | 6.6 |
| 39 | 4048 | 4.8 | - | - | 4559 | 6.0 | 4874 | 6.5 |

| | | | | | | | | |
|---|---|---|---|---|---|---|---|---|
| 40 | 4048 | 4.7 | - | - | 4559 | 5.8 | 4875 | 6.7 |
| 41 | 4049 | 4.8 | - | - | 4559 | 5.6 | - | - |
| 42 | 4050 | 5.0 | - | - | 4561 | 5.9 | - | - |
| 43 | 4051 | 4.9 | - | - | 4561 | 5.7 | - | - |
| 44 | 4053 | 5.1 | - | - | 4561 | 5.8 | - | - |
| 45 | 4054 | 5.0 | - | - | 4561 | 5.9 | - | - |
| 46 | 4055 | 4.9 | - | - | 4562 | 6.2 | - | - |
| 47 | 4056 | 4.8 | - | - | 4562 | 5.9 | - | - |
| 48 | 4063 | 4.8 | - | - | 4562 | 5.9 | - | - |
| 49 | - | - | - | - | 4563 | 5.8 | - | - |
| 50 | - | - | - | - | 4563 | 6.0 | - | - |
| 51 | - | - | - | - | 4563 | 5.7 | - | - |
| 52 | - | - | - | - | 4564 | 6.0 | - | - |
| 53 | - | - | - | - | 4565 | 6.2 | - | - |
| 54 | - | - | - | - | 4565 | 6.0 | - | - |
| 55 | - | - | - | - | 4565 | 5.8 | - | - |
| 56 | - | - | - | - | 4565 | 5.9 | - | - |
| 57 | - | - | - | - | 4565 | 5.8 | - | - |
| 58 | - | - | - | - | 4565 | 6.0 | - | - |
| 59 | - | - | - | - | 4566 | 6.0 | - | - |
| 60 | - | - | - | - | 4566 | 6.0 | - | - |
| 61 | - | - | - | - | 4566 | 5.9 | - | - |
| 62 | - | - | - | - | 4566 | 5.7 | - | - |
| 63 | - | - | - | - | 4566 | 5.9 | - | - |
| 64 | - | - | - | - | 4567 | 5.8 | - | - |
| 65 | - | - | - | - | 4571 | 6.0 | - | - |
| 66 | - | - | - | - | 4572 | 5.8 | - | - |
| 67 | - | - | - | - | 4574 | 5.7 | - | - |
| 68 | - | - | - | - | 4580 | 5.9 | - | - |
| # | 4875 < rpm ≤ 5125 | Power | 5125 < rpm ≤ 5375 | Pow er | 5375 < rpm ≤ 5625 | Power | 5625 < rpm ≤ 5875 | Power |
| 1 | 4864 | 6.3 | 5126 | 7.3 | 5417 | 8.5 | 5680 | 9.4 |
| 2 | 4869 | 6.5 | 5127 | 7.2 | 5418 | 8.3 | 5681 | 9.3 |
| 3 | 4873 | 6.1 | 5127 | 7.2 | 5419 | 8.9 | 5682 | 9.7 |
| 4 | 4876 | 6.5 | 5176 | 7.5 | 5419 | 7.8 | 5682 | 9.3 |
| 5 | 4878 | 6.6 | 5177 | 7.4 | 5422 | 8.2 | 5685 | 9.4 |
| 6 | 4880 | 6.7 | 5179 | 7.5 | 5428 | 7.0 | 5689 | 9.5 |
| 7 | 4881 | 6.8 | 5180 | 7.5 | 5520 | 8.6 | 5687 | 9.2 |
| 8 | 4882 | 6.7 | 5180 | 7.0 | 5529 | 8.4 | 5691 | 9.5 |
| 9 | 4882 | 6.5 | 5181 | 7.3 | 5531 | 8.8 | 5698 | 9.3 |
| 10 | 4884 | 6.6 | 5182 | 7.4 | 5569 | 9.0 | 5699 | 9.5 |
| 11 | 4886 | 6.7 | 5184 | 7.4 | 5571 | 8.5 | 5676 | 9.1 |

| | | | | | | | | |
|---|---|---|---|---|---|---|---|---|
| 12 | 4886 | 6.5 | 5185 | 7.1 | 5572 | 9.1 | 5679 | 9.5 |
| 13 | 4886 | 6.6 | 5185 | 7.4 | 5575 | 8.8 | 5682 | 8.5 |
| 14 | 4887 | 6.3 | 5187 | 7.4 | 5576 | 9.1 | 5681 | 11.0 |
| 15 | 4888 | 6.7 | 5232 | 7.8 | 5576 | 8.6 | 5680 | 7.9 |
| 16 | 4901 | 6.8 | 5233 | 7.6 | 5577 | 9.1 | 5679 | 8.5 |
| 17 | 4926 | 6.6 | 5236 | 7.6 | 5578 | 8.3 | 5683 | 8.0 |
| 18 | 4929 | 6.4 | 5236 | 7.9 | 5578 | 9.0 | 5684 | 8.9 |
| 19 | 4960 | 6.4 | 5237 | 7.7 | 5580 | 8.8 | 5685 | 9.3 |
| 20 | 4975 | 6.5 | 5237 | 7.8 | 5591 | 8.8 | 5686 | 9.5 |
| 21 | 4983 | 6.6 | 5238 | 7.6 | 5591 | 9.0 | 5692 | 10.1 |
| 22 | 4983 | 6.8 | 5238 | 7.9 | 5595 | 9.0 | 5690 | 9.7 |
| 23 | 4983 | 6.5 | 5239 | 7.6 | 5595 | 8.8 | 5691 | 9.1 |
| 24 | 4984 | 7.0 | 5240 | 7.7 | 5595 | 9.0 | 5695 | 8.5 |
| 25 | 4984 | 7.0 | 5242 | 7.6 | 5596 | 8.5 | 5696 | 8.5 |
| 26 | 4986 | 6.7 | 5247 | 7.8 | 5609 | 8.8 | 5699 | 9.6 |
| 27 | 4986 | 6.9 | 5248 | 7.7 | 5614 | 8.9 | 5701 | 9.1 |
| 28 | 4987 | 6.6 | 5248 | 7.6 | 5616 | 8.8 | 5703 | 9.3 |
| 29 | 4993 | 7.0 | 5249 | 7.7 | - | - | 5703 | 9.7 |
| 30 | 4993 | 6.8 | 5250 | 7.7 | - | - | 5768 | 10.4 |
| 31 | 4994 | 6.9 | 5251 | 7.6 | - | - | 5774 | 9.6 |
| 32 | 4998 | 6.8 | 5254 | 7.9 | - | - | 5789 | 10.0 |
| 33 | 4998 | 6.8 | 5254 | 8.2 | - | - | 5791 | 9.3 |
| 34 | 4999 | 6.7 | 5254 | 7.7 | - | - | 5795 | 9.1 |
| 35 | 5061 | 7.1 | 5254 | 7.6 | - | - | 5793 | 9.6 |
| 36 | 5062 | 6.8 | 5255 | 7.3 | - | - | 5796 | 10.0 |
| 37 | 5063 | 6.9 | 5256 | 7.8 | - | - | 5797 | 10.2 |
| 38 | 5066 | 6.8 | 5257 | 7.8 | - | - | 5801 | 9.3 |
| 39 | 5068 | 7.2 | 5257 | 7.7 | - | - | 5806 | 9.0 |
| 40 | 5070 | 7.1 | 5258 | 7.7 | - | - | 5810 | 8.5 |
| 41 | 5074 | 6.9 | 5258 | 7.3 | - | - | 5812 | 8.5 |
| 42 | 5079 | 7.0 | 5261 | 7.4 | - | - | 5811 | 10.5 |
| 43 | 5080 | 6.8 | 5262 | 7.8 | - | - | 5817 | 9.2 |
| 44 | 5085 | 7.1 | 5267 | 7.8 | - | - | 5815 | 8.7 |
| 45 | 5086 | 7.1 | 5268 | 7.6 | - | - | 5814 | 9.5 |
| 46 | 5088 | 6.9 | 5269 | 7.7 | - | - | 5821 | 8.5 |
| 47 | 5090 | 6.7 | 5269 | 7.6 | - | - | 5751 | 8.9 |
| 48 | 5091 | 7.1 | 5270 | 7.6 | - | - | 5753 | 9.7 |
| 49 | 5092 | 6.9 | 5273 | 7.5 | - | - | 5750 | 9.4 |
| 50 | 5096 | 7.1 | 5274 | 7.6 | - | - | 5749 | 9.1 |
| 51 | 5097 | 7.1 | 5275 | 8.1 | - | - | 5741 | 9.0 |
| 52 | 5099 | 7.0 | 5276 | 7.6 | - | - | 5746 | 9.0 |
| 53 | 5100 | 7.2 | 5276 | 7.9 | - | - | 5745 | 8.9 |

| | | | | | | | | |
|---|---|---|---|---|---|---|---|---|
| 54 | 5101 | 7.0 | 5277 | 7.6 | - | - | 5754 | 9.5 |
| 55 | 5103 | 7.0 | 5279 | 7.7 | - | - | 5753 | 9.3 |
| 56 | 5107 | 7.3 | 5342 | 8.2 | - | - | 5747 | 9.1 |
| 57 | 5108 | 7.4 | 5343 | 8.0 | - | - | 5741 | 8.7 |
| 58 | 5108 | 7.1 | 5349 | 7.9 | - | - | 5740 | 9.4 |
| 59 | 5121 | 7.2 | 5351 | 7.8 | - | - | 5742 | 9.1 |
| 60 | 5122 | 7.2 | 5353 | 8.0 | - | - | 5741 | 9.1 |
| 61 | 5122 | 7.4 | 5354 | 8.2 | - | - | 5740 | 9.3 |
| 62 | 5123 | 7.2 | 5359 | 7.9 | - | - | 5737 | 9.1 |
| 63 | 5124 | 7.2 | 5361 | 7.9 | - | - | 5738 | 9.1 |
| 64 | 5124 | 7.3 | 5362 | 7.9 | - | - | 5736 | 8.9 |
| 65 | - | - | - | - | - | - | 5732 | 9.1 |

| # | 5875 < rpm ≤ 6125 | Power | 6125 < rpm ≤ 6375 | Power | 6375 < rpm ≤ 6625 | Power |
|---|---|---|---|---|---|---|
| 1 | 5890 | 9.3 | 6126 | 10.5 | 6419 | 11.1 |
| 2 | 5893 | 9.5 | 6128 | 10.3 | 6466 | 12.1 |
| 3 | 5923 | 9.6 | 6129 | 10.5 | 6472 | 11.4 |
| 4 | 5928 | 9.5 | 6130 | 10.3 | 6473 | 11.1 |
| 5 | 5929 | 9.6 | 6136 | 10.5 | 6479 | 11.5 |
| 6 | 5930 | 9.6 | 6140 | 10.1 | 6483 | 11.7 |
| 7 | 5931 | 9.9 | 6144 | 10.1 | 6500 | 11.5 |
| 8 | 5932 | 9.6 | 6151 | 10.0 | 6511 | 11.9 |
| 9 | 5933 | 10.1 | 6153 | 10.5 | 6521 | 11.4 |
| 10 | 5933 | 9.9 | 6156 | 10.4 | 6529 | 12.3 |
| 11 | 5935 | 9.7 | 6210 | 10.5 | 6532 | 11.7 |
| 12 | 5937 | 9.6 | 6210 | 10.2 | 6542 | 12.1 |
| 13 | 5937 | 9.5 | 6211 | 10.5 | 6543 | 11.6 |
| 14 | 5937 | 9.7 | 6212 | 10.5 | - | - |
| 15 | 5938 | 9.4 | 6215 | 11.5 | - | - |
| 16 | 5939 | 9.4 | 6216 | 10.8 | - | - |
| 17 | 5939 | 9.8 | 6218 | 11.3 | - | - |
| 18 | 5939 | 9.2 | 6218 | 11.5 | - | - |
| 19 | 5940 | 9.9 | 6218 | 10.4 | - | - |
| 20 | 5940 | 9.6 | 6219 | 10.9 | - | - |
| 21 | 5941 | 9.7 | 6219 | 11.5 | - | - |
| 22 | 5942 | 10.7 | 6219 | 10.5 | - | - |
| 23 | 5942 | 10.1 | 6222 | 10.3 | - | - |
| 24 | 6008 | 10.4 | 6223 | 11.0 | - | - |
| 25 | 6009 | 10.9 | 6225 | 11.1 | - | - |
| 26 | 6009 | 10.3 | 6225 | 11.0 | - | - |
| 27 | 6010 | 10.8 | 6226 | 9.2 | - | - |
| 28 | 6010 | 9.6 | 6226 | 10.7 | - | - |
| 29 | 6011 | 9.6 | 6227 | 10.9 | - | - |

| | | | | | | |
|---|---|---|---|---|---|---|
| 30 | 6011 | 9.9 | 6229 | 10.9 | - | - |
| 31 | 6012 | 9.7 | 6229 | 10.7 | - | - |
| 32 | 6013 | 10.2 | 6230 | 11.3 | - | - |
| 33 | 6014 | 10.5 | 6230 | 11.7 | - | - |
| 34 | 6014 | 10.2 | 6230 | 11.8 | - | - |
| 35 | 6014 | 9.8 | 6230 | 10.9 | - | - |
| 36 | 6015 | 10.2 | 6230 | 10.5 | - | - |
| 37 | 6016 | 9.9 | 6230 | 10.3 | - | - |
| 38 | 6017 | 9.8 | 6231 | 11.3 | - | - |
| 39 | 6017 | 10.5 | 6232 | 12.7 | - | - |
| 40 | 6032 | 10.0 | 6233 | 11.2 | - | - |
| 41 | 6036 | 9.6 | 6233 | 11.3 | - | - |
| 42 | 6039 | 10.7 | 6233 | 10.6 | - | - |
| 43 | 6042 | 9.6 | 6234 | 12.4 | - | - |
| 44 | 6042 | 11.0 | 6237 | 10.1 | - | - |
| 45 | 6043 | 10.5 | 6240 | 10.8 | - | - |
| 46 | 6046 | 10.2 | 6242 | 11.3 | - | - |
| 47 | 6046 | 9.7 | 6243 | 10.2 | - | - |
| 48 | 6048 | 9.9 | 6244 | 11.2 | - | - |
| 49 | 6049 | 10.5 | 6246 | 10.2 | - | - |
| 50 | 6049 | 10.4 | 6263 | 10.7 | - | - |
| 51 | 6050 | 9.9 | 6266 | 11.2 | - | - |
| 52 | 6051 | 10.8 | 6274 | 10.8 | - | - |
| 53 | 6051 | 9.7 | 6277 | 10.2 | - | - |
| 54 | 6052 | 10.2 | 6278 | 11.0 | - | - |
| 55 | 6052 | 10.4 | 6280 | 11.8 | - | - |
| 56 | 6052 | 10.1 | 6285 | 10.7 | - | - |
| 57 | 6052 | 10.5 | 6290 | 11.2 | - | - |
| 58 | 6052 | 10.3 | 6291 | 11.2 | - | - |
| 59 | 6053 | 10.9 | 6293 | 10.7 | - | - |
| 60 | 6053 | 10.0 | 6294 | 11.0 | - | - |
| 61 | 6054 | 10.6 | 6295 | 10.7 | - | - |
| 62 | 6054 | 10.5 | 6297 | 11.1 | - | - |
| 63 | 6055 | 10.4 | 6297 | 11.9 | - | - |
| 64 | 6055 | 11.0 | 6298 | 11.2 | - | - |
| 65 | 6056 | 10.5 | 6362 | 11.2 | - | - |
| 66 | 6057 | 10.3 | 6367 | 10.7 | - | - |
| 67 | 6058 | 10.8 | 6367 | 10.7 | - | - |
| 68 | 6059 | 10.2 | 6368 | 11.5 | - | - |
| 69 | 6059 | 10.6 | - | - | - | - |
| 70 | 6059 | 10.4 | - | - | - | - |
| 71 | 6060 | 10.4 | - | - | - | - |

| | | | | | | |
|---|---|---|---|---|---|---|
| 72 | 6062 | 10.5 | - | - | - | - |
| 73 | 6062 | 10.5 | - | - | - | - |
| 74 | 6065 | 10.6 | - | - | - | - |
| 75 | 6066 | 9.5 | - | - | - | - |
| 76 | 6070 | 10.8 | - | - | - | - |
| 77 | 6071 | 10.5 | - | - | - | - |
| 78 | 6073 | 9.9 | - | - | - | - |
| 79 | 6075 | 9.6 | - | - | - | - |
| 80 | 6080 | 9.8 | - | - | - | - |
| 81 | 6081 | 9.9 | - | - | - | - |
| 82 | 6083 | 10.8 | - | - | - | - |
| 83 | 6083 | 10.0 | - | - | - | - |
| 84 | 6084 | 9.8 | - | - | - | - |
| 85 | 6085 | 10.2 | - | - | - | - |
| 86 | 6087 | 10.2 | - | - | - | - |
| 87 | 6093 | 10.6 | - | - | - | - |
| 88 | 6096 | 10.2 | - | - | - | - |
| 89 | 6097 | 10.2 | - | - | - | - |
| 90 | 6097 | 10.2 | - | - | - | - |

# Appendix 8: Determination of Power Efficiency

| Angular velocity (ω) | Power Efficiency (η) | Fractional uncertainty ($\frac{\Delta\eta}{\eta}$) | Absolute uncertainty ($\Delta\eta$) |
|---|---|---|---|
| $/rads^{-1}$ | $kgm^2s^{-3}$ | - | $kgm^2s^{-3}$ |
| 0 | 0 | 1.090 | 0 |
| 26 | 5.05041 | 1.492 | 7.53647 |
| 52 | 5.03806 | 1.497 | 7.54115 |
| 79 | 5.19595 | 1.501 | 7.79749 |
| 105 | 5.41957 | 1.504 | 8.15253 |
| 131 | 5.66842 | 1.508 | 8.54589 |
| 157 | 5.90947 | 1.511 | 8.92700 |
| 183 | 16.9106 | 1.582 | 26.7590 |
| 209 | 24.9627 | 1.622 | 40.4835 |
| 236 | 31.3804 | 1.651 | 51.8054 |
| 262 | 39.4344 | 1.685 | 66.4387 |
| 288 | 48.5075 | 1.722 | 83.5170 |
| 314 | 54.8055 | 1.748 | 95.8195 |
| 340 | 56.5343 | 1.760 | 99.5000 |
| 367 | 56.0104 | 1.765 | 98.8327 |
| 393 | 54.6171 | 1.766 | 96.4554 |
| 419 | 53.4560 | 1.767 | 94.4715 |
| 445 | 50.8639 | 1.764 | 89.7014 |
| 471 | 49.2979 | 1.763 | 86.8983 |
| 497 | 47.8633 | 1.761 | 84.2870 |
| 524 | 47.4140 | 1.762 | 83.5577 |
| 550 | 47.6857 | 1.765 | 84.1640 |
| 576 | 48.2416 | 1.769 | 85.3168 |
| 602 | 49.3993 | 1.774 | 87.6109 |
| 628 | 50.3016 | 1.777 | 89.4075 |
| 655 | 51.2764 | 1.782 | 91.3497 |
| 681 | 52.3214 | 1.786 | 93.4234 |
| 707 | 53.1726 | 1.789 | 95.1214 |

# Appendix 9: Arduino Code for Modulating Motor RPM

```
Int VoltPin = A0; int
SignalPin = 9; int readVal;
float Volt;
#include <Servo.h> Servo
ESC;

void setup()
{ ESC.attach(9,1000,2000);
Serial.begin(9600);
}
void loop() {
realVal = analogRead(VoltPin); realVal =
map(realVal, 0, 1023, 0 180); ESC.write(realVal);
}
```

## 【評語】100042

The author studied the relationship between the angular velocity and power efficiency of a twin-blade helicopter during hovering. The issue is properly addressed and proper analysis methodology is carried out for the modeling and simulation of the problem based on empirical data. However, the additional issues about the relationship between the thrust or the blade angle vs. the power efficiency still required further study. It is suggested that the additional issues should be taken into account so as to improve the project.